Modeling crustal deformation and rupture processes related to upwelling of deep CO_2-rich fluids during the 1965-1967 Matsushiro Earthquake Swarm in Japan

Frédéric Cappa[1,2], Jonny Rutqvist[2] and Koji Yamamoto[3,4]

[1] Lawrence Berkeley National Laboratory, Earth Sciences Division, Berkeley, USA

[2] GeoAzur (UMR6526), University of Nice Sophia-Antipolis, Côte d'Azur Observatory, Sophia-Antipolis, France

[3] Mizuho Information and Research Institute, Tokyo, Japan

[4] Japan Oil, Gas and Metals National Corporation, Tokyo, Japan

* Corresponding author. Fax: (+ 33) 4.92.94.26.10

E-mail address: cappa@geoazur.unice.fr (F. Cappa); jrutqvist@lbl.gov (J. Rutqvist)

Running title: **THE MATSUSHIRO EARTHQUAKE SWARM**

Submitted to: **JOURNAL OF GEOPHYSICAL RESEARCH**

F. Cappa, GeoAzur (UMR6526), University of Nice Sophia-Antipolis, Côte d'Azur Observatory, 250 rue Albert Einstein, Les Lucioles 1, 06560 Sophia-Antipolis, France (cappa@geoazur.unice.fr)

J. Rutqvist, Earth Sciences Division, Lawrence Berkeley National Laboratory, 1 Cyclotron Rd., MS 90-1116, Berkeley, CA 94720, USA. (jrutqvist@lbl.gov)

K. Yamamoto, Mizuho Information and Research Institute, 3-1 Kanda-Nishikicho, Chiyoda-ku, Tokyo 101-0054, Japan.

Abstract

[1] In Matsushiro, central Japan, a series of more than 700,000 earthquakes occurred over a 2-year period (1965-1967) associated with a strike-slip faulting sequence. This swarm of earthquakes resulted in ground surface deformations, cracking of the topsoil, and enhanced spring-outflows with changes in chemical compositions as well as carbon dioxide (CO_2) degassing. Previous investigations of the Matsushiro earthquake swarm have suggested that migration of underground water and/or magma may have had a strong influence on the swarm activity. In this study, employing coupled multiphase flow and geomechanical modelling, we show that observed crustal deformations and seismicity can have been driven by upwelling of deep CO_2-rich fluids around the intersection of two fault zones—the regional East Nagano earthquake fault and the conjugate Matsushiro fault. We show that the observed spatial evolution of seismicity along the two faults and magnitudes surface uplift, are convincingly explained by a few MPa of pressurization from the upwelling fluid within the critically stressed crust—a crust under a strike-slip stress regime near the frictional strength limit. Our analysis indicates that the most important cause for triggering of seismicity during the Matsushiro swarm was the fluid pressurization with the associated reduction in effective stress and strength in fault segments that were initially near critically stressed for shear failure. Moreover, our analysis indicates that a two order of magnitude permeability enhancement in ruptured fault segments may be necessary to match the observed time evolution of surface uplift. We conclude that our hydromechanical modelling study of the Matsushiro earthquake swarm shows a clear connection between earthquake rupture, deformation, stress, and permeability changes, as well as large-scale fluid flow related to degassing of CO_2 in the shallow seismogenic crust. Thus, our study provides further evidence of the important role of deep fluid sources in earthquake fault dynamics and surface deformations.

INDEX TERMS: 8010 Structural Geology: Fractures and faults; 7209 Seismology: Earthquake dynamics and mechanics; 8045 Structural Geology: Role of fluids; 8159 Tectonophysics: Evolution of the Earth: Rheology—crust and lithosphere; 5139 Physical Properties of Rocks: Transport properties; *KEYWORDS:* Earthquake swarm; Deep CO_2 fluids; Deformation; Rupture; Effective stress; Hydromechanical modelling.

1. Introduction

[2] Earthquakes are among the most dynamic geological events, and associated ruptures provide a dramatic manifestation of the Earth's internal activity. Earthquakes involve a variety of coseismic and postseismic responses, in which rock deformations and stress changes can provide insight into crustal strength. Moreover, earthquakes may be correlated to pore-pressure transients [*Byerlee*, 1990; *Rice*, 1992; *Spicak and Horalek*, 2001; *Miller*, 2002; *Miller et al.*, 2004; *Hainzl*, 2004] that may reduce crustal strength and promote a great number of earthquakes with a large range of magnitudes [*Roeloffs*, 2000; *Manga and Wang*, 2007]. The hypothesis is that an increase in fluid pressure reduces the effective normal stress, effectively weakening the fault and shear strength to a level below the prevailing shear stress. Coseismic and postseismic mechanisms can induce observable surface deformations, pore pressures and seismic signatures that can be used to constrain numerical models. Such models enable greater understanding of the underlying mechanisms, including rupture, and the permeability and strength evolution of the both the earth's crust and earthquake faults. Because of the potentially key role of fluids in fault dynamics, it is important better describe coupled pore pressure, deformation and stress changes in faults, thereby improving our ability to forecast earthquakes.

[3] The 1965-1967 Matsushiro earthquake swarm in the Chubu district of southwest Honshu, near Nagano city, central Japan (36°32'N, 138°12'E) (Figure 1a), represents a good opportunity to analyze these hydromechanical interactions over a long period of intense seismic activity. This was one of the most energetic swarms in the world, and many types of geophysical observations have been carried out at the site [*Matsu'ura and Karakama*, 2005]. A series of more than 700,000 earthquakes (i.e, approximately 60,000 earthquakes were felt, and about 640,000 unfelt tremors were recorded) occurred over a 2-year period during a strike-slip faulting sequence, resulting in ground-surface deformations and cracking of the

topsoil and enhanced spring-outflows, with changes in chemical composition and carbon dioxide (CO_2) degassing (Figure 1-3) [*Hagiwara and Iwata*, 1968; *Japan Meteorological Agency*, 1968; *Kisslinger*, 1975]. The highest magnitude reached M_w = 5.4, and epicentral depths ranged from near surface to 12 km, with an average depth of 4–5 km. The total energy released by the earthquakes in this period was calculated to be 1.66×10^{21} Joules (Figure 3b), equivalent to a single earthquake of magnitude 6.3 [*Hagiwara and Iwata*, 1968]. The earthquake swarm sequence occurred on subvertical strike-slip faults, migrating from northeast (NE) to southwest (SE) along an elliptic area of about 34 km in length and 18 km in width (Figure 1a), and from near surface to about 12 km-depth (Figure 1b) [*Hagiwara and Iwata*, 1968]. The swarm was accompanied by seismic focal area expansion and large crustal uplift [*Ohtake*, 1976]. The Matsushiro seismic region, as defined by the hypocenters of the earthquakes recorded during the swarm (Figure lb), is contained entirely within the central belt of uplift, a relatively homogeneous diorite intrusion which crosses the southwestern part of Honshu Island [*Ohtake*, 1976]. When the swarm occurred, large amounts of groundwater were expelled in the uplifted area, accompanied by free gases, such as CO_2 and CH_4 as well as increased NaCl concentration [*Yoshida et al.*, 2003]. Structural geology and geophysical observations [*Nakamura and Tsuneishi*, 1967; *Kasahara*, 1970; *Tsuneishi and Nakamura*, 1970; *Nur*, 1974; *Kisslinger*, 1975; *Stuart and Johnston*, 1975] indicated that the earthquakes nucleated along a portion of the Matsushiro fault zone with a left-lateral strike-slip faulting, and occurring in three principal episodes (Figure 1 and 3a-b):

- During the first year, earthquakes occurred near Mt. Minakami, which is a Pleistocene andesite volcano. Low-level activity (micro-earthquakes) started in August, 1965, reached a broad peak in November, and subsided gradually. During this period, earthquakes occurred at shallow depths, from the sub-surface to 8 km depth.

- Then, earthquakes occurred in the southwestern and northeastern regions within the area. This growth in the source region was believed to be caused by a dextral strike-slip faulting on the conjugate East Nagano fault [*Kisslinger*, 1975]. This second-most-active episode began in mid-March 1966, peaked in April 1966 with some 7,000 recorded events per day, and again subsided during the summer of 1966.
- The third and last episode started in early August 1966 and peaked in late August and September. Then, the activity gradually diminished to low levels by the end of 1967.

[4] In addition, Oike and Taniguchi [*1988*] demonstrated four patterns of earthquake activity at Matsushiro: *(1)* isolated large events, *(2)* large mainshock suddenly followed by many smaller aftershocks, *(3)* swarms composed of many shocks including a few large shocks, and *(4)* swarms composed of many shocks but no conspicuously large shocks.

[5] Among a variety of geophysical observations made during the Matsushiro earthquake swarm, analyses of seismicity, surface levelling, spring-flow, and chemistry data have shown:

- A strong local uplift of about 0.75 m on the fault trace in the original swarm region, when seismic activity was at its highest (Figure 2a);
- A strike-slip zone (Matsushiro fault) of approximately 5 to 7 km in length, with an estimated offset of 1 to 2 m at the ground surface (Figure 2a and 3c);
- A fault dilation of about 0.3 m at the ground surface (Figure 3c);
- Numerous individual *en echelon* ground cracks with strike-slip of up to 0.3 m (Figure 2b) [*Nakamura and Tsuneishi*, 1967];
- Enhanced spring-outflows of deep origin brine water (i.e, NaCl) saturated with CO_2 (Figure 2a and 3d) [*Yoshida et al.*, 2003]. This surface expulsion corresponded to approximately 1×10^7 m^3 of mineral water discharged in one year from the uplifted area, preferentially through faults and newly formed cracks [*Tsuneishi and Nakamura*, 1970].

[6] Figures 3c-d show that the rate of surface displacements and water outflow is discontinuous with rapidly accelerated stages associated with changes in seismic activity. After the 1-year period of water expulsion, spring outflow rapidly decreased, and the surface subsided slowly after reaching this peak, levelling off with a maximum residual uplift of about 0.4 to 0.6 m by the middle of 1968. This outflow has been interpreted as resulting from the collapse of a focal region with a dilatant strain of about 10^{-4} [*Nur*, 1974] as well as seismic pumping [*Sibson et al.*, 1975]. Note that analyses of the Matsushiro groundwater chemical composition notably indicated that CO_2, which was the major component of the gas, originated from the mantle, and that CH_4, another major component, originated from thermal decomposition of organic materials contained in sedimentary rocks [*Yoshida et al.*, 2003]. Given these data, the Matsushiro earthquake swarm was thought to be strongly related to the upwelling of overpressured water with dissolved CO_2 into the upper crust, inducing dilatancy in the fault-crust system [*Asano et al.*, 1969; *Nur*, 1974; *Kisslinger*, 1975]; a correlation between earthquakes and the peaks of dilatational strain was observed. Thus, these previous studies at Matsushiro suggest a strong coupling among stress, multiphase fluids, and structural dynamic responses.

[7] An overpressuring from upwelling of deep CO_2-rich fluid appears to be a reasonable hypothesis for earthquake initiation [*Spicak and Horalek*, 2001; *Brauer et al.*, 2003; *Chiodini et al.*, 2004; *Miller et al.*, 2004; *Hainzl*, 2004; *Giammanco et al.*, 2008]. Such overpressuring has also been identified recently as a driving mechanism for an earthquake sequence in northern Italy [*Miller et al.*, 2004] and Sicily [*Giammanco et al.*, 2008]. This hypothesis is further supported by seismotectonic analyses and seismic tomography near Matsushiro in the Niigata Prefecture [*Mogi*, 1988; *Sibson*, 2008; *Xia et al.*, 2008], and geophysical observations during fluid-injection experiments conducted at Matsushiro in the mid-1970s [*Ohtake*, 1970]. The injection experiments were conducted at about 2 km depth by injecting water directly into

the Matsushiro fault. After a first injection lasting a few days and a subsequent peak in induced seismicity, a second massive injection test indicated a substantial increase in fault permeability. During the second injection, induced seismicity spread several kilometres downwards along the fault plane within a few months. The injection pressure stabilized at an overpressure of a few MPa, despite increasing injection rates. The induced seismicity and associated permeability changes indicates that the injection resulted in shear reactivation and dilation of pre-existing fractures within intensively fractured rock in the damaged rock zone adjacent to the fault plane. The relatively low overpressure needed for inducing seismicity and shear induced permeability enhancement indicates that fractures were initially near critically stressed for shear failure.

[8] Alternative causes for the observed induced seismicity at Matsushiro have also been suggested. For example, Oike and Taniguchi [*1988*] suggested that tidal effects influence the periodicity of earthquake activity at Matsushiro. They observed synchronized occurrences of shocks with tidal phases over several days. Triggering of earthquakes by such earth tides was thought to occur only at the critical stress level of the host rock. Several investigators [*Nur*, 1974; *Stuart and Johnston*, 1975; *Kisslinger*, 1975] have also attributed the onset of the swarm with a magmatic intrusion beneath the Mount Minakami volcano. Others [*Nakamura and Tsuneishi*, 1966; *Matsuda*, 1967; *Kasahara*, 1970; *Tsuneishi and Nakamura*, 1970] proposed that the swarm accompanied the formation of a new fault zone, driven by regional compressional stresses, in an area with no evidence of a pre-existing fault and little seismicity before 1965.

[9] Although the temporal characteristics of Matsushiro earthquake activities have been investigated [*Matsu'ura and Karakama*, 2005], the spatiotemporal interactions between fluid pressure, stress, deformation, rupture zones and the evolution of hydraulic and strength properties in the fault-crust system have not been investigated to date in a fully coupled

numerical analysis. Several studies at other sites have shown that when fluids propagate through a fault zone the evolution of hydromechanical properties play a key role in the fault instability processes [*Parotidis et al.*, 2005; *Cappa et al.*, 2007; *Guglielmi et al.*, 2008; *Cappa*, 2009]. Fluids may also have an important role in explaining episodes of the fault-strength recovery between earthquakes [*Hickman et al.*, 1995]. Moreover, at Matsushiro, the region of water outflow, uplift, faulting and seismicity closely coincide in space—likely reflecting their link through hydromechanical interactions (Figure 2a). One remarkable feature of earthquake swarms is that they tend to expand focal areas. However, their occurrence patterns vary greatly, and their generation mechanisms have not been understood completely [*Aoyama et al.*, 2002].

[10] In this paper, we investigate the role of upwelling deep CO_2-rich fluids in triggering earthquakes and crustal deformations during the Matsushiro earthquake swarm. We employ 3D coupled multiphase fluid flow and geomechanical modelling to investigate how pressure transients of upwelling CO_2-rich fluids and fault rupture with permeability enhancement may be linked to the observed evolution of earthquake hypocenters, surface deformations, and the chemical evolution of springwater. The central part of our analysis is the coupled hydromechanical interaction of two faults (the regional East Nagano fault and the conjugate Matsushiro fault) that intersect at the centre of the swarm initiation in 1965. It is our hypothesis that the intersection of the two faults may have provided a conduit for upwelling deep CO_2-rich magmatic brine water. We use the 2 year time-series observations of surface displacements and hypocenter locations to constrain the numerical model and to analyze how earthquake ruptures occurred under certain physical conditions. The spatiotemporal characteristics of the rupture initiation and propagation are investigated through the fluid diffusion process in the earthquake faults and surrounding crust. Unlike the previous work on this earthquake swarm, we give special attention to interactions between deformation and

rupture zones, as well as stress and fluid transfer in the fault system for the upper 6 km of the seismogenic crust. Through our numerical investigations, we show that the rupture sequence and surface displacements are caused by pressurization from upwelling CO_2-rich fluids in a critically stressed crust—under a strike-slip regime near the frictional limit. Moreover, we found a consistent pore-pressure and deformation transient signal that indicates a strong hydromechanical coupling, with a two-orders-of-magnitude increase in fault permeability, during rupture.

2. Modelling set-up

2.1 Numerical analysis method

[11] To investigate the effects of a deep CO_2-fluid source on initiation and propagation of rupture along the Matsushiro and the conjugate East Nagano seismogenic faults, we employed three-dimensional, coupled multiphase brine-CO_2 flow and geomechanical modelling. The goal was to simulate the general hydromechanical field responses, as observed in Figures 1 to 3. For that, the TOUGH-FLAC code [*Rutqvist et al.*, 2002] was used. TOUGH-FLAC is based on the coupling of a finite-difference geomechanical code, FLAC^{3D} [*Itasca*, 2006] and a finite-volume multiphase flow code, TOUGH2 [*Pruess et al.*, 1999]. This code allows a detailed evaluation of the hydromechanical effects on rupture initiation and propagation, and was recently used to study the effects of CO_2 motion within faulted and tectonically active formations [*Rutqvist et al.*, 2007; *Rutqvist et al.*, 2008]. It has also been applied to study coupled CO_2 fluid upwelling, surface uplift and geomechanical changes at the Phlegrean Fields, Italy [*Todesco et al.*, 2004].

[12] The code simulates the fluid-flow and deformation-coupled processes of discrete faults embedded in porous media. For the flow problem, TOUGH-FLAC solves the multiphase

version of the diffusion equation (Eq. 1). Each fluid component is accumulated from relevant contributions in each phase, χ ($\chi = g$ for gas and $\chi = l$ for liquid).

$$\frac{\partial(\phi\rho_\chi S_\chi)}{\partial t} = \nabla\cdot\left[\rho_\chi k\left(\frac{k_{r\chi}}{\mu_\chi}\right)\left(\nabla P_\chi - \rho_\chi g\nabla z\right)\right] + \rho_\chi q_\chi, \qquad \chi = l, g \tag{1}$$

in which ϕ is the porosity, ρ_χ the density, S_χ the saturation, t the time, k the intrinsic permeability, $k_{r\chi}$ the relative permeability of each phase, μ_χ the viscosity, P_χ the pressure, g the gravity, z the elevation, and q_χ a source term. Relative permeability of gas and liquid phases was calculated from Corey's function [*Corey*, 1954], while capillary pressure was governed by the van Genuchten's function [*van Genuchten*, 1980]. Among the possible equations-of-state modules available in the TOUGH2 multiphase flow simulator for modeling of brine-CO_2 mixtures, the EWASG module was selected [*Pruess et al.,* 1999]. This module is applicable for the wide range of temperature and pressure considered in this study (i.e., from ground surface to a depth of 6000 m), but otherwise has a less complete description of thermo-physical properties of CO_2-brine mixtures than alternative modules such as ECO2N [*Pruess,* 2005].

[13] The multiphase flow processes calculated with TOUGH2 are coupled with the geomechanical processes calculated in FLAC^{3D} by direct pore-volume coupling and indirect coupling through mechanically induced permeability changes [*Rutqvist et al.*, 2002; *Todesco et al.*, 2004]. Most importantly, a change in pore pressure in TOUGH2 is linked to FLAC^{3D} through the effective stress law, and a change in stress or strain in FLAC^{3D} is linked to TOUGH2 through a permeability change law. In this study, we used a fault permeability model in which fault intrinsic permeability changes with volumetric strain (dilatancy), such that for a fully reactivated fault (maximum volumetric strain), permeability increases by two orders of magnitude; a reasonable value for a change in fault seismogenic permeability

[*Sibson and Rowland*, 2003; *Mitchell and Faulkner*, 2008]. In this fault permeability model, the permeability changes, k/k_0, are related to the volumetric strain, ε_v, according to:

$$k = k_o \cdot (1 + \beta \cdot \Delta\varepsilon_v) \tag{2}$$

in which k_0 is the initial (pre-swarm) permeability.

[14] In the numerical analyses conducted herein, the rock matrix behaves as an elastic material, whereas faults are governed by an elasto-plastic constitutive law. The faults zones are envisioned to include a 100 m thick fault damage zone consistent with intensively fractured rocks on each side of the central fault plane. The choice of 100 m wide damage zone is supported by geological observations at Matsushiro [*Hagiwara and Iwata*, 1968; *Ohtake*, 1974], and also has geological support for other major fault zones in the world [*Mitchell and Faulkner, 2009*]. The failure and inelastic deformations in the intensively fractured zone are evaluated using an isotropic elasto-plastic Mohr-Coulomb model. An inelastic slip state is reached when the shear stress acting on a fracture plane within the intensively fractured zone exceeds its shear strength, governed by a Coulomb criterion:

$$\tau = c + \mu_s (\sigma_n - P) \tag{3}$$

where τ is the critical shear stress for rupture occurrence, c is the cohesion, μ_s is the static friction coefficient, and σ_n is the normal stress.

2.2 Geometry, initial conditions and deep fluid source function

[15] We modelled a three-dimensional representation (100 × 100 × 6 km) of the Matsushiro site, including the Matsushiro fault and the conjugate East Nagano fault (Figure 4). The East Nagano fault is a regional active fault zone along which earthquakes have been recorded since the 1800s, whereas the Matsushiro fault was unknown prior to the 1960s earthquake swarm. The spatial distribution of earthquake hypocenters and the observed shear offset during the Matsushiro swarm indicated that the fault or the ruptured part of the fault is about 5 km long.

At 6 km depth, the bottom of the model is located just below the extent of the earthquake hypocenters during Stage 1 of the swarm (Figure 3b), which may indicate the depth of the Matsushiro fault or its ruptured part. During Stages 2 to 4, earthquake activities along the East Nagano fault extend below 6 km, which means that the model captures the upper seismogenic zone of this fault. The two intersecting fault zones were discretized into solid elements of 200 m in thickness, to include intensively fractured (damaged) rock zone adjacent to the central fault plane. The numerical grid was refined near the fault zone, with grid sizes gradually increasing towards the lateral model boundaries.

[16] In-situ and boundary fluid pressures were set according to the initial hydrostatic pressure gradient. The model was initially saturated with brine water in a liquid phase. We assume an initial NaCl concentration of 1.5 g/L as observed in the field before the beginning of the earthquake swarm (Figure 3d). Temperature was set according to a constant geothermal depth gradient based on well logging data. Displacement normal to the lateral and bottom boundaries was fixed to zero. The ground surface was free to move.

[17] An initial in-situ stress regime was imposed consistent with the dominant crustal strike-slip stress regime of central Japan and the observed strike-slip faulting induced during the main shock at Matsushiro. The maximum principal horizontal stress was set to be greater than the vertical stress, in itself greater than the least principal horizontal stress ($\sigma_{Hmax} > \sigma_V > \sigma_{hmin}$). In such a case, fault reactivation occurs when the difference between σ_{Hmax} and σ_{hmin} is sufficiently large. Jaeger and Cook [*1979*] showed that the limiting ratio of maximal principal effective stress, $\sigma_1' = \sigma_1 - \alpha P$ (α is the Biot's coefficient, Biot [*1941*]), and the minimum principal effective stress at depth, $\sigma_3' = \sigma_3 - \alpha P$, is given by:

(4)

where q is the limiting stress difference (slope of the σ_1' versus σ_3' line). For our study, μ_s was set to 0.6; thus, a q value of 3.13, a lower limit value frequently observed in studies of the correlation between active fault zones and maximum shear stress [*Byerlee*, 1978; *Sibson and Rowland*, 2003]. Note that Equation (4) is valid for the isotropic Mohr-Coulomb model corresponding to the intensively fractured rock of random oriented fractures, and in which shear takes place along a fracture with an optimum orientation for shear failure. According to the orientation of the stress field and faults in the model, the optimum orientation is parallel to the two conjugate fault zones. This is also consistent with statistical studies of focal mechanism at the site [*Ichikawa*, 1967]. In addition to this hypothesis, we also assumed that the horizontal stress at the ground surface is not zero, but applied a small compressive horizontal stress of 0.75 MPa added to the initial in-situ stress regime.

[18] After computing the initial state, we injected brine water and CO_2 at 6 km depth into a point source (1 km^2) located at the intersection of the two faults and its neighbourhood. This source represents the supply of upwelling CO_2-rich brine water that may have originated from a magmatic source deeper then 10 km and migrated along the intersection of the two faults. The injected water contains 5 g/L of NaCl, and a 5% mass fraction of CO_2. The fluid temperature was 190 °C. A constant flow rate of 9,000 L/min was imposed at the source at 6 km depth. This source rate was estimated from observed increases in surface discharges and further calibrated to obtain a maximum overpressure of about 2 MPa at around 2 km depth, consistent with the maximum overpressure observed towards the end of the 1970s massive fault injection test [*Ohtake*, 1974]. The applied rate of 9,000 L/min is higher than the estimated maximum discharge rate at the ground surface of 1,500 to 2,000 L/min (Figure 3d), which is reasonable since much of the upwelling water spread laterally along the faults.

[19] Model results were compared to the observed evolution of vertical and horizontal displacements and chemical concentrations at the ground surface, and to the seismicity pattern

(epicentral areas) at depth. We did not attempt to make an exact match of simulated and observed data but rather tried to obtain a reasonable agreement to the general evolution and magnitude of data presented in Figure 2a and 3c. Consequently, we did not simulate each stage of decelerated-accelerated uplift and displacement related to the three peaks of seismic activity shown in Figure 3.

2.3 Material properties of reference model

[20] The rock properties of the faults and surrounding crust have a great impact on the complex coupled hydromechanical and chemical transport evolution of the system. Based on geophysical investigations at the site, the crustal rock mass is divided into a low-velocity surface layer (0 to 1,500 m depth) and a high-velocity base layer (below 1,500 m) [*Japan Meteorological Agency*, 1968]. We first conducted a large number of test simulations and sensitivity studies with varying material properties over a reasonable range. Based on a model calibration constrained by observations from the various field observations and geophysical measurements, we then defined a set of reference model parameters with the property values listed in Table 1.

[21] The values of Young's modulus for the high and low velocity zone listed in Table 1 are about 60% of the dynamic properties estimated from sonic velocity profiles. This is reasonable, considering the known difference between static and dynamic elastic properties. The Young's modulus of the fault zone is lower than that of the surrounding crust, also reasonable considering the increased fracturing and damaged rock around fault zones. This change in Young's modulus close to the fault is also supported by laboratory data for major fault zones, like the Caleta Coloso fault, a 5-km-offset strike-slip fault in the Atacama fault system of northern Chile [*Faulkner et al.*, 2006]. The permeability of the crustal rock is reasonable for a sparsely fractured rock, whereas the initial permeability of the fault zones is similar to a more intensively fractured media. The initial (prerupture) fault permeability was

taken from estimates derived from the 1970s fault injection experiment described in Section 1. These values are reasonable for seismogenic permeability [*Sibson and Rowland*, 2003; *Talwani* et al., 2007]. Moreover, at the intersection of the two faults, we applied a higher initial permeability ($k_o = 5 \times 10^{-15}$ m^2), necessary for matching Cl evolution at the ground surface as well as matching the extent of the uplift bulge centred around the fault intersection. In general, an increased permeability at the fault intersection could be expected as a result of increased damage and fracturing in this area.

3. Modelling results

3.1 Sensitivity to source pressure, permeability, and stress

[22] In this section, we study hydromechanical responses of the system related to the evolution of fluid pressure at the source, as well as the changes in fault permeability and the σ_1' to σ_3' ratio. In this sensitivity analysis, we mainly focus on the evolution of fluid pressure and chemical concentration at the source, as well as surface uplift and spring-water chlorine concentration (Figure 3c-d).

3.1.1 Effects of pressure change at the source

[23] Model results show that source pore pressure increase rapidly from the very outset of the constant rate injection (Figure 5a). The rapid pressure buildup is followed by a slow increase to steady-state, and after terminating the injection at 1 year, the pressure progressively reduces to values slightly above the initial hydrostatic state. Thus, at the source, the pressure increased by 3.5 MPa in 11 days, then continued to increase at a slower rate to reach a steady-state maximum overpressure of 4.4 MPa. This pressure increase is directly accompanied by an increase in volumetric strain, which corresponds to an expansion (Figure 8b). The strain magnitude at the source reached 0.5×10^{-3} during the rapid pressure increase, and 1.75×10^{-3} at 1 year.

[24] Figures 5b-d present the evolution of effective stress state (i.e., the stress path) at different depths along the intersection of the two faults. The failure criterion of Eq. (4) indicates that onset of shear failure would occur if $\sigma_1' \geq 3.13\sigma_3'$. Figure 5b shows that the stress path for a point just above the source (i.e., at 5.75 km depth) reaches this limit after 23 days when pressure change was near its maximum ($\Delta P \sim 4$ MPa). Then, rupture progresses upwards along the fault and reaches 3 km depth after 81 days, and the ground surface after 114 days (Figure 5c-d).

[25] Model results also reproduce the observed uplift magnitude and evolution (Figure 6a). The calculated uplift magnitude is equivalent to the measured one, with a peak value of 0.76 m at 1 year, and a residual value of 0.57 m at 2 years.

[26] The results also showed that Cl and CO_2 concentrations increase quickly at the source (Figure 5a) and reach the ground surface in about 9 months (Figure 6). The evolution of Cl in Figure 6a is similar to the observed evolution of Cl concentration in Figure 3d. Vertical profiles presented in Figure 6b indicate that Cl concentration progressively increase from the source to the ground surface and reach a maximal value in the entire fault intersection after 21 months. This means that Cl concentration continues to increase during the pressure fall-off.

3.1.2 Effect of change in fault permeability

[27] The influence of changes in fault permeability was examined by varying the value of the β-parameter in Equation (2). Results show that the hydromechanical response is very sensitive to changes in fault permeability (Figure 7a). A good agreement with the measured surface uplift was obtained for a change in fault permeability of two orders of magnitude (i.e, $k/k_o = 100$). When a smaller change in permeability was assumed, uplift magnitude was overestimated, and the curve shape was not reproduced during the pressure decrease stage. Thus, the strain-induced permeability changes during fault rupture within the faults have a

significant impact on the hydromechanical responses of rock mass during fault pressurisation and subsequent pressure recovery.

3.1.3 Effect of stress ratio (σ_1'/σ_3')

[28] The effects of stress ratio the between σ_1' and σ_3' on the hydromechanical response of the faults were examined by comparing three models, in which the stress ratio was varied from a noncritical (σ_1'/σ_3' = 1.4 and 2) to a critical stress regime (σ_1'/σ_3' = 3.13). Model results show a good fit to surface uplift (Figure 7b) was obtained only for an initial stress field near frictional limit, assuming σ_1'/σ_3' = 3.13 as a critical stress regime. In that case, a strike-slip stress regime was estimated, with $\sigma_{Hmax} = 1.339 \times \sigma_V$ and $\sigma_{hmin} = 0.7 \times \sigma_V$ (σ_V being lithostatic), and assuming the orientation of σ_{Hmax} is N090, so that it corresponds to an azimuth of 48° from the East Nagano fault, towards the South (see the stress ellipsoid in Figure 4). When a smaller stress ratio was assumed, no rupture occurs along the faults (Figure 7b) and values of uplift were underestimated, because in these cases the system remains elastic, with no rupture and associated plastic straining.

3.2 Reference model

[29] A described in Section 2, we calibrate the model input parameters to achieve a reasonable agreement to the observed evolution of seismicity, surface uplift and chemical concentration. The key parameters for this calibration are the injection rate at the source, the stress regime, set to a critical stress ratio of σ_1'/σ_3' = 3.13, and the fault permeability and its changes during rupture estimated to a factor of 100. To analyze this best match (calibrated) solution in detail, we examine a series of vertical profiles of change in fluid pressure, permeability, strain and stress (Figure 8). The vertical profiles are located at the centre of the model, where the Matsushiro and East Nagano faults intersect. Profiles are presented at different times during the simulation. In addition, we also present the distribution of changes in fluid pressure and volumetric strain at 6 km depth at 1 year (Figure 9), the spatial evolution

of changes in fluid pressure and shear strain along the earthquake faults (Figure 10 to 13) at different times, and surface displacements at 1 year (Figure 14).

3.2.1 Fault hydromechanical behaviour

[30] Figure 8a shows that pressure spreads rapidly along the faults and propagates from the source region towards the surface after 1 month. At 1 year, the pressure gradient peaks with a pressure increase of 4.4 MPa near the source. At 2 years, an overpressure of about 0 to 2 MPa is maintained along the faults.

[31] This change in pressure is accompanied by changes in volumetric strain and vertical displacement (Figure 8b-c). After 1 month of fluid upwelling, there is an increasing (elastic) volumetric strain from the deep source region towards the surface. From 1 to 6 months, the volumetric strain and uplift increases dramatically over the entire 6 km depth of the fault. This increased volumetric strain is the result of elastic volumetric strain caused by increased fluid pressure in both the fault and surrounding crust, as well as plastic volumetric strain during progressive failure along the fault (see Figure 5b-d). After 6 months, the fluid pressure within the fault is more or less constant, but an additional volumetric strain and uplift occurs as a result of lateral diffusion of fluid pressure and poroelastic expansion in the surrounding crust. After termination of the deep source injection, the pressure decreases rapidly, whereas volumetric strain and vertical displacement decrease only slightly. The remaining volumetric strain after 2 years is permanent plastic strain, whereas the remaining uplift is also affected by the remaining pressure increase in the surrounding crust.

[32] Figure 8d shows the evolution of fault permeability calculated from the volumetric strain according to Equation (2) with $\beta = 3 \times 10^4$. A two order of magnitude permeability increase occurs for the fully reactivated fault, which is consistent with values estimated in-situ by Ohtake [*1976*] ($k \sim 9.86 \times 10^{-15}$ m^2 to 9.86×10^{-14} m^2). This permeability change influences

the diffusion of pore pressure, and can be related to the expansion speed of seismicity along the faults.

[33] Figures 8e and 8f indicate that pore pressure rise induces a lowering of effective stress normal to the fault plane of several MPa, but only a slight increase in shear stress (of a few tens of kPa). This means that failure is mainly related to the lowering of effective stress, effectively weakening the faults. At the bottom, the effective normal stress is lowered by about 2 MPa whereas the fluid pressure increased by 4 MPa. This shows that the total stress normal to the fault plane is increased by $\Delta\sigma_n = \Delta\sigma'_n + \Delta P = 2 + 4 = 2$ MPa as a results of poroelastic stress.

3.2.2 3D spatiotemporal change of pore-pressure and deformations within the earthquake faults and its surroundings

[34] Our modelling results show that the pressure changes caused by the deep fluid source are rapidly distributed in the faults, accompanied by slow diffusive leakage from the faults to the neighbouring low-permeable crust (Figure 9a-10 and 12). During the pressure-increase stage, pressure diffuses both upward and laterally in the faults, with the pressure gradient decreasing from the source to the surrounding areas, inducing a progressive increase in shear strain along these planes. Shear strain follows a complex pattern (Figure 11 and 13).

[35] Figure 9a shows that the pressure increase at 6 km depth affects a large zone that extends several kilometers from the pressurization source. This pressure buildup is accompanied by an increase in volumetric strain in a zone smaller than that of the pressure change. Near the source, this expansion is strongly guided by the faults, along which strain is higher than in the crust (Figure 9b).

[36] Inside the faults, pore pressure progressively increases to 4.4 MPa at 1 year near the fluid source (Figure 10 and 12). Along the Matsushiro fault, pressure increase affects the entire

fault (30 km^2) after 6 months, whereas along the East Nagano fault, pressure increase affects a greater area (132 km^2), laterally limited to about 10 km on both sides of the source region.

[37] The fluid pressure rise is accompanied by shear strain, with maximum shear strain mainly localized where the faults intersect and particularly near the surface where shearing is less restricted (Figure 11 and 13). Along the Matsushiro fault, shear strain increases near the source during the first 1 month of fluid upwelling, and then intense shearing propagates towards the surface with the highest magnitude reaching 2.1×10^{-3} at 1 year. Laterally, shear strain is limited on both sides of the source at about 1.4 km. Along the East Nagano fault, shear strain followed the same path, but the lateral extent is much greater.

[38] During the first three months, the fluid pressure migration acts (1) to induce earthquakes along its path, and (2) to induce poroelastic strain and displacement towards the surface. After this period, CO_2-rich fluid penetrates the entire upward portions of the faults with pore pressure high enough to dilate rocks and to extrude fluids to the ground surface. When pressure decreases, shear strain along the fault and crustal dilatation decreases. The time for diffusion of pressurized fluids controls the time to expand the swarm area.

3.2.3 Surface displacements

[39] Consistent with levelling surveys at the site (Figure 2a), a maximum uplift of about 0.75 m was calculated at the intersection between the two faults after 1 year of fluid upwelling, when the pressure is the highest (Figure 14a). Results also show that the observed extent of the uplift area is reproduced by the model. Indeed, the simulated uplift area extends to about 10 km in the strike direction of the East Nagano fault and about 7 km in the strike direction of the Matsushiro fault.

[40] Distribution of the uplift follows a square pattern at the faults intersection showing strong influence of fault deformation. When pressure decreases, the surface subsided, levelling off with a residual uplift of about 0.57 m at the fault intersection.

[41] Maximum horizontal surface displacements calculated along the faults are presented in Figure 14b. Results show an asymmetric displacement field around the fault traces, with zones of inverse motion appearing on both sides of the Matsushiro and East Nagano faults. These displacements indicate a strike-slip motion consistent with geophysical observations. Near the fault intersection, the calculated maximum shear displacement is about 0.95 m along both faults (Figure 14b). This is consistent with distribution shear strain calculated on planes (Figure 11 and 13). The observed hypocenter locations also correlate well with areas of the largest displacements and shear strain, particularly in the area of the two faults.

[42] In summary, both vertical and horizontal surface displacements are localized within a dilatant zone of several kilometres around where the faults intersect. Dilatancy is mainly related to fault shear motion and poroelastic strain in the country rock surrounding the faults. In that zone, the dilatancy process can induce cracking of the top soil such as those observed in the field during the swarm.

3.3 Rupture propagation model during the Matsushiro earthquake swarm

[43] Figure 15 shows the spatiotemporal evolution of rupture zones along the faults during the 2-year simulation. We may compare this simulated evolution of the rupture zone with the observed evolution of earthquake hypocenters shown in Figure 1. Consistent with observed earthquake evolution, our analysis shows that rupture is first initiated along the Matsushiro fault, and then along the East Nagano fault. On the Matsushiro fault, rupture starts near the fluid source and then propagates from the bottom to the ground surface within six months. Along the East Nagano fault, rupture starts in the lower portion after three months and propagates both laterally and upwards during the 1-year fluid pressurization. For our simulated 1 year fluid upwelling, rupture zones along the East Nagano fault stop nucleating at about 10 km on each side of the central fault intersection (Figure 15).

[44] Our analysis shows that ruptures primarily occur in zones of increased pressure, but also propagate above the pressurized zone where initial stresses are low. Localized concentration of stresses as well as pressure induced localized effective stress releases triggers shear failure, particularly in areas where the faults intersect. The shear failure results in shear dilation that may induce a significant permeability increases along the faults.

4. Discussion

4.1 Contribution of pore-pressure diffusion and tectonic stress state to earthquake triggering

[45] In this study, we suggest that observed crustal deformations and seismicity at Matsushiro could have been driven by the upwelling of deep CO_2-rich fluids around the intersection of two fault zones. We showed that the rupture sequence of the two faults, as observed from the spatial evolution of seismicity as well as the observed magnitude of surface uplift could be a results of pressurization of only a few MPa in excess of hydrostatic. A rupture for such a low pressure change is possible within a critically stressed crust—a crust under a strike-slip stress regime near the frictional strength limit [*Townend and Zoback*, 2000]. Thus, our analysis demonstrates that the most important cause of seismic activity at Matsushiro was the pore-pressure transients associated with the upwelling of CO_2-rich fluids, reducing the effective stress and shear strength sufficiently to induce rupture and seismicity. The rupture and seismicity associated with shear dislocation of pre-existing fractures within an intensively fractured fault rock may result in a significantly increased permeability that will accelerate the process.

[46] The effects of the fluid source gradually propagated to the surrounding areas. In the shallow parts of the faults, fault rupture may have been assisted by the initial deeper crustal movements and associated shear stress transferred towards the ground surface. Nevertheless,

the swarm was initially triggered by the effects of pore-pressure change around the intersection between the Matsushiro and East Nagano earthquake faults, and then expanded. The inferred magnitude overpressure of about 4 MPa at the fluid source is subject to some uncertainty, because a reasonable good match to field observations may also be obtained if applying a higher overpressure and if at the same time adjusting other parameters such as rock deformation modulus. In the study of earthquake faulting at Colfiorito, Italy, by Miller et al. [*2004*], a substantially higher overpressure was inferred. However, applying such a high overpressure in the Matsushiro case would be inconsistent with field observations in the 1970s massive water injection test. The 1970s injection test indicated that the fault could not sustain an overpressure of more than a few MPa (an overpressure relative to the initial hydrostatic pressure cause by the active injection).

4.2 Relation between the evolution of seismicity and hydromechanical changes

[47] Our hydromechanical analysis of the Matsushiro earthquake swarm shows a strong correlation between the spatial distributions of observed earthquake hypocentres and simulated fluid pressure-induced fault rupture. Consequently, we can hypothesize that the spatial evolution seismicity was related to the upwelling and lateral migration of large volume CO_2-rich fluids. Other factors also contributing to the evolution of seismicity may include variation of initial crustal stress as well as heterogeneity of crustal properties such as permeability, porosity, and strength. The hypocenter migration can be explained by underground fluid diffusion and associated poroelastic stress transferred upward and laterally from the source region to surrounding areas. Thus, the temporal pattern of seismicity is limited by the velocity of pore-pressure diffusion and stress transfer. We emphasize that in complex, highly fractured media, poroelastic and elastic interactions act together in promoting seismicity and controlling its spatial and temporal pattern.

[48] In this study we focused on the diffusion of underground fluid as the dominant factor in triggering the earthquakes. Other potentially important factors such as stress and strain accumulations from historic earthquakes, stress corrosion processes, interaction among earthquakes, and passage of waves were not considered. Here, we mainly focused on the migration of multiphase fluid, assuming that the fluctuation of seismicity probably reflects the transient pore pressure variation around the source as indicated by previous studies [*Nur*, 1974; *Sibson et al.*, 1975; *Ohtake*, 1976]. For simplicity, we assumed a single fluid source at 6 km depth, although a more wide spread upwelling may have occurred from depth greater than 10 km. Moreover, the time evolution of the fluid upwelling was simplified neglecting effects from an oscillating upwelling rate. In addition to these mechanical effects, the mechano-chemical processes could also play a significant role during the seismic cycle [*Blanpied et al.*, 1992; *Beeler and Hickman*, 2004; *Gratier and Gueydan*, 2007]. Gratier and Gueydan [2007] discussed the importance of these mechano-chemical interactions, within characteristic time intervals, on the weakening and strengthening of faults in the upper crust. Moreover, experimental studies of permeability variations in fresh fractures at seismogenic temperatures have shown permeability can significantly recover over similar timescales of days to weeks [*Morrow et al*, 2001], and microfractures on the order of hours to days [*Brantley et al*, 1990]. Consequently, competing fracturing and sealing processes at different scales will control fault zone fluid flow and a variety of geological processes.

[49] Future studies will address heterogeneities related to multiple pressurization sources and fluid flow-induced oscillations, mechano-chemical effects, as well as transient stress changes caused by dynamic effects (i.e., seismic waves propagation) on coupled hydromechanical processes. Detection of changes in poroelastic parameters, on the basis of simultaneous and high-frequency measurements of fluid pressures and mechanical displacements in deep boreholes (combined with seismological, geodetic, electromagnetic and geochemical

measurements at ground surface), may be useful in forecasting the strength state of the upper crust and the environmental impact of shallow earthquakes.

5. Conclusion

[50] In this paper, we investigated the role of upwelling deep CO_2-rich fluids in the triggering of earthquakes and crustal deformations during the 1965-1967 Matsushiro earthquake swarm, in Japan. We employed 3D coupled multiphase fluid flow and geomechanical modelling to investigate how pressure transients from upwelling CO_2-rich fluids and fault rupture with permeability enhancement may be linked to the observed evolution of earthquake hypocenters, surface deformations, and the chemical evolution of spring water. The central part of our analysis is the coupled hydromechanical interaction of two faults (the Matsushiro fault and the East Nagano fault) that intersect at the centre of a seismic swarm initiation in 1965. It was our hypothesis that the intersection of the two faults may have provided a conduit for upwelling, CO_2-rich, deep magmatic brine water. In our modelling, the upwelling CO_2-rich fluid was simulated by a fluid source at the fault intersection at a depth of 6 km, which is at the bottom boundary of our model.

[51] Our results, which are in qualitative agreement with field observations, suggest that seismic swarm activity is strongly related to underground fluid migration. The spatial relation between simulated rupture zones and observed earthquake hypocentres in this region suggests that the seismicity may be triggered by fluid-pressure migration through their mechanical interactions with the tectonic stress field. Moreover, pore-pressure distribution influences how the poroelastic stress transfer can be accumulated near the strained fault zones and trigger shallow seismicity near the surface.

[52] We have shown that spatiotemporal variations in the rupture zones at Matsushiro are consistent with a transient increase in fluid pressure, and a rupture primarily initiated along

the Matsushiro fault, near the pressurization source, and then, laterally along the conjugate East Nagano fault. This is consistent with the hypocenter locations inferred from geophysical surveys of this earthquake swarm. Moreover, the simulated surface uplift magnitude and lateral extent are consistent with that inferred from levelling observations. The fact that the uplift bulge does not extend laterally more than about 5 km supports our hypothesis of fluid upwelling initially concentrated along the intersection of the two faults. In the present study, we did not attempt to match each stage of the time evolution of uplift (i.e., accelerating and decelerating stages), which would require the time-varying source rate to reflect episodes of CO_2-rich fluids expelled from the deep source. However, our analysis provides a reasonable evaluation of available field data.

[53] The potential for rupture at Matsushiro strongly depended on the magnitude and orientation of the initial stress field. A strike-slip faulting stress regime, near the frictional limit and oriented N090, was estimated to reproduce the seismicity pattern (epicentral areas) and surface displacements. Because the tectonic stress field is near its frictional limit, an overpressure (of a few MPa) of the upwelling CO_2-rich fluids was sufficient to trigger the earthquake swarm. Moreover, our models indicated that another significant factor is the change in fault permeability related to fault rupture. Our analysis suggests that an increase in fault permeability of two orders of magnitude in ruptured areas of the fault may be necessary to explain these data. Thus, the in-situ stress regime, as well as fault strength and permeability, are likely the most important parameters that control the nucleation, propagation, arrest, and occurrence of the earthquake swarm during its 2 year migration through the seismogenic crust.

[54] Our hydromechanical model simulation shows the link between earthquake rupture, stress and permeability changes, and large-scale fluid flow related to degassing of CO_2 in the shallow seismogenic crust. Fluid upwelling and associated hydromechanical effects can play a

dominant role in promoting earthquakes during a seismic sequence. At Matsushiro, fluid pressure may have triggered micro-earthquakes by the formation or reactivation of small fractures, which could in turn trigger larger earthquakes in subsequent stages. Consequently, hydromechanical couplings are important processes in seismology that can influence the short-term periodicities in earthquake distributions within an entire time-series analysis. The evolution of permeability with deformations that depend on the effective stress conditions provide a conceptual basis for the interpretation of observed response characteristics. On the basis of these models, direct observations of the surface deformations above seismically active zones should improve our ability to forecast earthquakes. The study also indicates that surface deformation may be used for monitoring, as a precursor for surface CO_2 leakage associated with large-scale underground CO_2 storage.

Acknowledgments

[55] The work presented in this paper was financed by the Ministry of Economy, Trade and Industry Ministry (METI) of Japan. Further funds for completing this paper were provided by the Assistant Secretary for Fossil Energy, Office of Natural Gas and Petroleum Technology, through the National Energy Technology Laboratory, under the U.S. Department of Energy Contract No. DE-AC02-05CH11231. The authors acknowledge the advice from the Technical Advisory Committee members and colleagues of the Natural Analogue Study for CO2 Geological Sequestration. The authors are grateful for the constructive comments and recommendations by the associate editor, Dan Faulkner at the University of Liverpool, and for the editorial review by Dan Hawkes at the Lawrence Berkeley National Laboratory, and an external technical review by Giovanni Chiodini at the National Institute of Geophysics and Volcanology, Napoli, and one unidentified reviewer, which substantially improved this paper.

References

Aoyama, H., M. Takeo, and S. Ide (2002), Evolution mechanisms of an earthquake swarm under the Hida Mountains, central Japan, in 1998, *J. Geophy. Res.*, *107*(B8) doi:10.1029/2001JB000540.

Asano, S., S. Kubota, H. Okada, M. Nogoshi, H. Suzuki, K. Ichikawa, and H. Watanabe (1969), Explosion seismic studies of the underground structure in the Matsushiro Earthquake Swarm Area, *J. Phys. Earth*, *17*(1),77-90.

Beeler, N.M., and S.H. Hickman (2004), Stress-induced time-dependent fracture closure at hydrothermal conditions, *J. Geophys., Res*, 109, B02211, doi:10.1029/2002JB001782.

Biot, M.A. (1941), General theory of three-dimensional consolidation, *J. Appl. Phys.*, *12*,155–164

Blanpied, M.L., D.A. Lockner, and J.D. Byerlee (1992), An earthquake mechanism based on rapid sealing of faults, *Nature*, 358(6387), 574-576.

Brantley, S.L., Evans, B., Hickman, S.H. & Crerar, D.D, 1990. Healing of microcracks in quartz – implications for fluid flow, *Geology*, **18**(2), 136-139.

Brauer, K., H. Kampf, G. Strauch, and S.M. Weise (2003), Isotopic evidence ($^{3}He/^{4}He$, $^{13}CO_2$) of fluid-triggered intraplate seismicity, *J. Geophys. Res.*, 108 (B2), 2070, doi:10.1029/2002JB002077

Byerlee, J.D. (1978), Friction of rocks, *Pure Appl. Geophys.*, *116*, 615-626.

Byerlee, J.D. (1990), Friction, overpressure, and fault normal compression, *Geophys. Res. Lett.*, *17*, 2109–2112.

Cappa, F., Y. Guglielmi, and J. Virieux (2007), Stress and fluid transfer in a fault zone due to overpressures in the seismogenic crust, *Geophys. Res. Lett.*, *34*, L05301, doi:10.1029/2006GL028980.

Cappa, F. (2009), Modeling fluid transfer and slip in a fault zone when integrating heterogeneous hydromechanical characteristics in its internal structure, *Geophys. J. Int.* (in press)

Chiodini, G., C. Cardellini, A. Amato, E. Boschi, S. Caliro, F. Frondini, and G. Ventura (2004), Carnon dioxide Earth degassing and seismogenesis in central and southern Italy, *Geophys. Res. Lett.*, L07615, doi:07610.01029/02004GL019480

Corey, A.T. (1954), The interrelation between oil and gas relative permeabilities, *Producers Monthly*, 38-41.

Davies, J.P., and D.K. Davies (1999), Stress-dependent permeability: characterization and modelling, *Society of Petroleum Engineers*, SPE paper 56813, 429-444.

Faulkner, D.R., T.M. Mitchell, D. Healy, and M.J. Heap (2006), Slip on 'weak' faults by the rotation of regional stress in the fracture damage zone, *Nature*, 444(7121), 922-925.

Giammanco, S., M. Palano, A. Scaltrito, L. Scarfi, and F. Sortino (2008), Possible role of fluid overpressure in the generation of earthquake swarms in active tectonic areas: The case of the Peloritani Mts. (Sicily, Italy), *Journal of Volcanology and Geothermal Research*, 178, 795-806.

Guglielmi Y., F. Cappa, and D. Amitrano (2008), High-definition analysis of fluid-induced seismicity related to the mesoscale hydromechanical properties of a fault zone, *Geophys. Res. Lett.*, *35*, L06306, doi:10.1029/2007GL033087.

Hagiwara, T., and T. Iwata (1968), Summary of the seismographic observation of Matsushiro swarm earthquakes, *Bull. Earthq. Soc. Amer.*, *46*, 485-515.

Hainzl, S. (2004), Seismicity patterns of earthquake swarms due to fluid intrusion and stress triggering, *Geophys. J. Int.*, 159, 1090-1096.

Hickman, S., R. Sibson, and R. Bruhn (1995), Introduction to special section: Mechanical involvement of fluids in faulting, *J. Geophys. Res*., *100*, 12831–12840.

Ichikawa, M. (1967), Statistical studies of the focal mechanism of Matsushiro earthquake swarm, *Zisin, Ser. II*, 20 116-127 (in Japanese).

Itasca Consulting Group (2006), FLAC^{3D}, Fast Lagrangian Analysis of Continua in 3 Dimensions, Version 2.0. Five volumes, Minneapolis, Minnesota, Itasca Consulting Group.

Japan Meteorological Agency (1968), Report on the Matsushiro earthquake swarm, August 1965 December 1967, *Technical Report of the Japan Meteorological Agency*, 125-137.

Jaeger, J.C., and N.G.W. Cook (1979), Fundamentals of rock mechanics, ed. Third edition, New York: Capman 1 Hall, p. 590.

Kasahara, K. (1970), The source region of the Matsushiro swarm earthquakes: *Tokyo Univ. Earthquake Research Inst. Bull.*, *48*, p. 581-602.

Kisslinger, C. (1975), Processes during the Matsushiro, Japan, Earthquake Swarm as Revealed by Leveling, Gravity, and Spring-Flow Observations, *Geology*, 57-62.

Manga, M., and C.Y. Wang (2007), Earthquake hydrology, In: *Treatise on Geophysics*, G. Schubert editor, *4*, 293-320.

Matsuda, T. (1967), Geological aspect of the Matsushiro earthquake fault. *Bull. Earthquake Res. Inst., Tokyo Univ., 45*, 537-550.

Matsu'ura, R., and I. Karakama (2005), A point-process Analysis of the Matsushiro Earthquake Swarm Sequence: The Effect of Water on Earthquake Occurrence, *Pure Appl. Geophys., 162*, 1319-1345, doi:10.1007/s00024-005-2672-0.

Miller, S.A. (2002), Properties of large ruptures and the influence of fluids on earthquakes and faulting, *J. Geophys. Res.*, *107*, B9, 2182, doi:10.1029/2000JB000032.

Miller, S.A., C. Collettini, L. Chiaraluce, M. Cocco, M. Barchi, and B.J.P. Kaus (2004), Aftershocks driven by a high-pressure CO_2 source at depth, *Nature*, *427*, 724-727.

Mitchell, T.M., and D.R. Faulkner (2008), Experimental measurements of permeability evolution during triaxial compression of initially intact crystalline rocks and implications for fluid flow in fault zones, *J. Geophys. Res.*, 113(B11412, doi:10.1029/2008JB005588)

Mitchell, T.M., and D.R. Faulkner (2009), The nature and origin of off-fault damage surrounding strike-slip fault zones with a wide range of displacements: a field study from the Atacama fault system, northern Chile, *J. Struct. Geol.*, doi:10.1016/j.jsg.2009.05.002, in press.

Mogi, K (1988), The mechanism of the occurrence of the Matsushiro earthquake swarm in central Japan and its relation to the 1964 Niigata earthquake, *Tectonophysics*, 159, 109:119.

Morrow, C.A., D.E Moore, and D.A. Lockner (2001), Permeability reduction in granite under hydrothermal conditions, *J. Geophys. Res.*, **106**(B12), 30551-30560.

Nakamura, K., and Y. Tsuneishi (1966), Ground cracks at Matsushiro probably of underlying strike-slip origin. I, Preliminary report, *Bull. Earthquake Res. Inst., Tokyo Univ.*, *44*, 1371-1384.

Nakamura, K., and Y. Tsuneishi (1967), Ground cracks at Matsushiro probably of underlying strike-slip fault origin, II: The Matsushiro earthquake fault: *Tokyo Univ. Earthquake Research Inst. Bull.*, *45*, 417-471.

Nakamura, K. (1971), Matsushiro jishin kara mananda koto, *Kagaku Asahi*, *10*, 127-133.

Nur, A. (1974), Matsushiro, Japan, Earthquake Swarm: Confirmation of the Dilatancy-Fluid Diffusion Model, *Geology*, 217-221.

Ohtake, M. (1974), Seismic activity induced by water injection at Matsushiro, Japan, *J. Phys. Earth.*, *22*,163-176.

Ohtake, M. (1976), A review of the Matsushiro earthquake swarm, *Kagaku*, *46*, 306–313, (in Japanese).

Oike, K., and K. Taniguchi (1988), The relation between seismic activities and earth tides in the case of the Matsushiro earthquake swarm, *Bull. Diss. Prev. Inst., Kyoto Univ.*, *38*, Part 1 No. 331, 17–28.

Parotidis, M., S.A. Shapiro, and E. Rothert (2005), Evidence for triggering of the Vogtland swarms 2000 by pore pressure diffusion, *J. Geophys. Res.*, *110*, B05S10, doi:10.1029/2004JB003267.

Pruess, K., C. Oldenburg, and G. Moridis (1999), TOUGH2 user's guide, version 2.0. *Lawrence Berkeley National Laboratory Report*, LBNL-43134, Berkeley.

Pruess, K. (2005), ECO2N—a TOUGH2 fluid property module for mixtures of water, NaCl, and CO2, *Lawrence Berkeley National Laboratory Report*, LBNL-57952, Berkeley, California.

Rice, J. (1992), Fault stress states, pore pressure distribution, and the weakness of the San Andreas Fault, In: *Faults Mechanics and Transport Properties of Rocks* (eds Evans B, Wong TF), 475-503, Academic Press, London.

Roeloffs, E. (2000), The Parkfield, California earthquake experiment: An update in 2000, *Current Science*, *79*, 1226-1236.

Rutqvist, J., Y-S. Wu, C-F. Tsang, and G. Bodvarsson (2002), A modeling approach for analysis of coupled multiphase fluid flow, heat transfer, and deformation in fractured porous rock, *Int. J. Rock Mech. Min. Sci.*, *39*, 429-442.

Rutqvist, J., J. Birkholzer, F. Cappa, and C-F. Tsang (2007), Estimating maximum Sustainable injection pressure during geological sequestration of CO_2 using coupled fluid flow and geomechanical fault-slip analysis, *Energy Conv. Man., 47*, 1798-1807.

Rutqvist, J., J.T. Birkholzer, and C-F. Tsang (2008), Coupled reservoir-geomechanical analysis of the potential for tensile and shear failure associated with CO_2 injection in multilayered reservoir-caprock systems, *Int. J. Rock Mech. Min. Sci.*, 45**,** 132-143.

Sibson, R.H., J. McM. Moore, and A.H. Rankin (1975), Seismic pumping—a hydrothermal fluid transport mechanism, *Jl. geol. Soc. Lond.*, *131*, 653-659.

Sibson, R.H., and J.V. Rowland (2003), Stress, fluid pressure and structural permeability in seismogenic crust, North Island, New Zealand, *Geophys. J. Int.*, *154*, 584-594.

Sibson, R.H. (2007), An episode of fault-valve behaviour during compressional inversion? The 2004 M_J6.8 Mid-Niigata Prefecture, Japan, earthquake sequence, *Earth and Planetary Science Letters*, 257, 188-199.

Spicak, A., and J. Horalek (2001), Possible role of fluids in the process of earthquake swarm generation in the West Bohemia/Vogtland seismoactive region, *Tectonophysics*, 336, 151-161.

Spycher, N., K. Pruess, and J. Ennis-King (2003), CO2-H2O mixtures in the geological sequestration of CO2. I. Assessment and calculation of mutual solubilities from 12 to 100°C and up to 600 bar, *Geochim. Cosmochimi. Acta*, *67*(16), 3015-3031.

Stuart, W.D., and M.J.S. Johnston (1975), Intrusive origin of the Matshshiro Earthquake Swarm, *Geology*, 63-67.

Talwani, P., L. Chen, and K. Gahalaut (2007), Seismogenic permeability, k_s, *J. Geophys. Res.*, *112*, B07309, doi:10.1029/2006JB004665.

Todesco, M, J. Rutqvist, G. Chiodini, K. Pruess, and C. Oldenburg (2004), Modeling of recent volcanic episodes at Phlegrean Fields (Italy): geochemical variations and ground deformation, *Geothermics*, 33, 531-547.

Townend, J. and M.D. Zoback (2000), How faulting keeps the crust strong, *Geology*, 28(5), 399-402.

Tsukahara, H., and N. Yoshida (2005), Origin of groundwater which caused the Matsushiro earthquake swarm. *Chikyu*, 27/6, 453-460 (in Japanese).

Tsuneishi, Y., and K. Nakamura (1970), Fault associated with the Matsushiro swarm earthquake, *Tokyo Univ. Earthquake Research Inst. Bull.*, *48*, p. 29.

van Genuchten, M.T. (1980), A closed-form equation for predicting the hydraulic conductivity of unsaturated soils, *Soil Sci. Soc. Am. J.*, *44*:892–8.

Xia, S., D. Zhao and Q. Xuelin (2008), The 2007 Niigata earthquake: Effect of arc magma and fluids, Physics of the Earth and Planetary Interiors, 166, 153-166.

Yoshida, N., H. Tsukahara, and T. Okusawa (2003), Andesitic Magmatic Water Which Generated Matsushiro Earthquake Swarm And S Wave Reflector, *AGU Fall Meeting*, V52B-0437.

Figure captions

Figure 1. (a) Tectonic features and time series of epicentral areas [*Ohtake*, 1976], and (b) earthquakes swarm migration [*Hagiwara and Iwata*, 1968].

Figure 2. (a) Areas of maximum uplift, horizontal displacements and water discharge induced in September 1966 during the Matsushiro earthquake swarm [after Japan *Meteorological Agency*, 1968; *Nakamura*, 1971]; (b) ground cracks *en echelon* developed on the northeastern side of Mt. Minakami from the spring to the autumn 1966 [after *Nakamura*, 1971].

Figure 3. (a) Number of earthquakes during the swarm migration; (b) mean depth of focal points and seismic energy release; (c) uplift and fault motions; (d) spring-water outflow and chloride [Cl^-] concentration. [after *Kasahara*, 1970; *Tsuneishi and Nakamura*, 1970; *Tsukahara and Yoshida*, 2005].

Figure 4. Model geometry including the Matsushiro and East Nagano earthquake faults. Stress orientation for the reference model.

Figure 5. (a) Calculated evolution change in fluid pressure and [Cl^-] and [CO_2] concentration at the source located at 6 km depth, and effective principal stress path at (b) 5.75 km, (c) 3.25 km, (d) 0.25 km depth at the intersection between the Matsushiro and East Nagano faults.

Figure 6. (a) Calculated uplift and [Cl^-] and [CO_2] concentration at the ground surface (at the intersection between the Matsushiro and East Nagano faults); (b) vertical profiles of change in [Cl^-] content over the 2 year period.

Figure 7. Calculated surface uplift at the fault intersection for different (a) permeability changes, (b) stress ratio (σ_1'/σ_3'), and (c) effective stress paths near the source for different stress ratio.

Figure 8. Vertical profiles of changes in (a) fluid pressure, (b) volumetric strain, (c) shear displacement, (d) permeability (bold black line corresponds to the initial permeability at the fault intersection, $k_o = 5 \times 10^{-15}$ m^2), (e) effective normal stress, and (f) shear stress. Profiles are taken at the intersection between the Matsushiro and East Nagano faults.

Figure 9. Change in (a) fluid pressure and (b) volumetric strain at 6 km-depth.

Figure 10. Change in fluid pressure calculated within the Matsushiro fault plane at different times. CO_2 source is located at x = 0, z = 6 km.

Figure 11. Change in shear strain calculated within the Matsushiro fault plane at different times. The CO_2-rich fluid source is located at x = 0, z = 6 km.

Figure 12. Change in fluid pressure calculated within the East Nagano fault plane at different times. The CO_2-rich fluid source is located at x = 0, z = 6 km.

Figure 13. Change in shear strain calculated within the East Nagano fault plane at different times. The CO_2-rich fluid source is located at x = 0, z = 6 km.

Figure 14. Map and close-up view of (a) calculated maximum uplift and (b) horizontal displacements at the ground surface for a stress ratio (σ_1'/σ_3') of 3.13.

Figure 15. Calculated distribution of rupture zones at different times along the Matsushiro and East Nagano earthquake faults.

Table 1. Material parameters

Parameters	Faults	Crust
Young's modulus, E, (GPa)	5.74	6.7* and 14.73**
Poisson's ratio, ν, (-)	0.1875	0.1875
Density, ρ, (kg/m^3)	2500	2500
Static friction coefficient, μ_s, (-)	0.6	-
Dilation angle, ψ, (deg.)	20	-
Biot's coefficient, α, (-)	1	1
Initial intrinsic permeability, k_o, (m^2)	1×10^{-16}	1×10^{-18}
Initial porosity, ϕ_o, (-)	0.05	0.01
Residual porosity, ϕ_R, (-)	0.04	0.009
Corey irreducible gas saturation, S_{rg}, (-)	0.05	0.05
Corey irreducible liquid saturation, S_{lr}, (-)	0.3	0.3
van Genuchten (1980) capillary strength parameter, Pc_0, (kPa)	19.9	3100
van Genuchten (1980) exponent, m, (-)	0.457	0.457
Initial [Cl^-] concentration (g/l)	1.5	1.5
Initial [CO_2] concentration (g/l)	0	0

* Value for the 1.5 km-thick surface layer; ** value for the 4.5 km-thick base layer

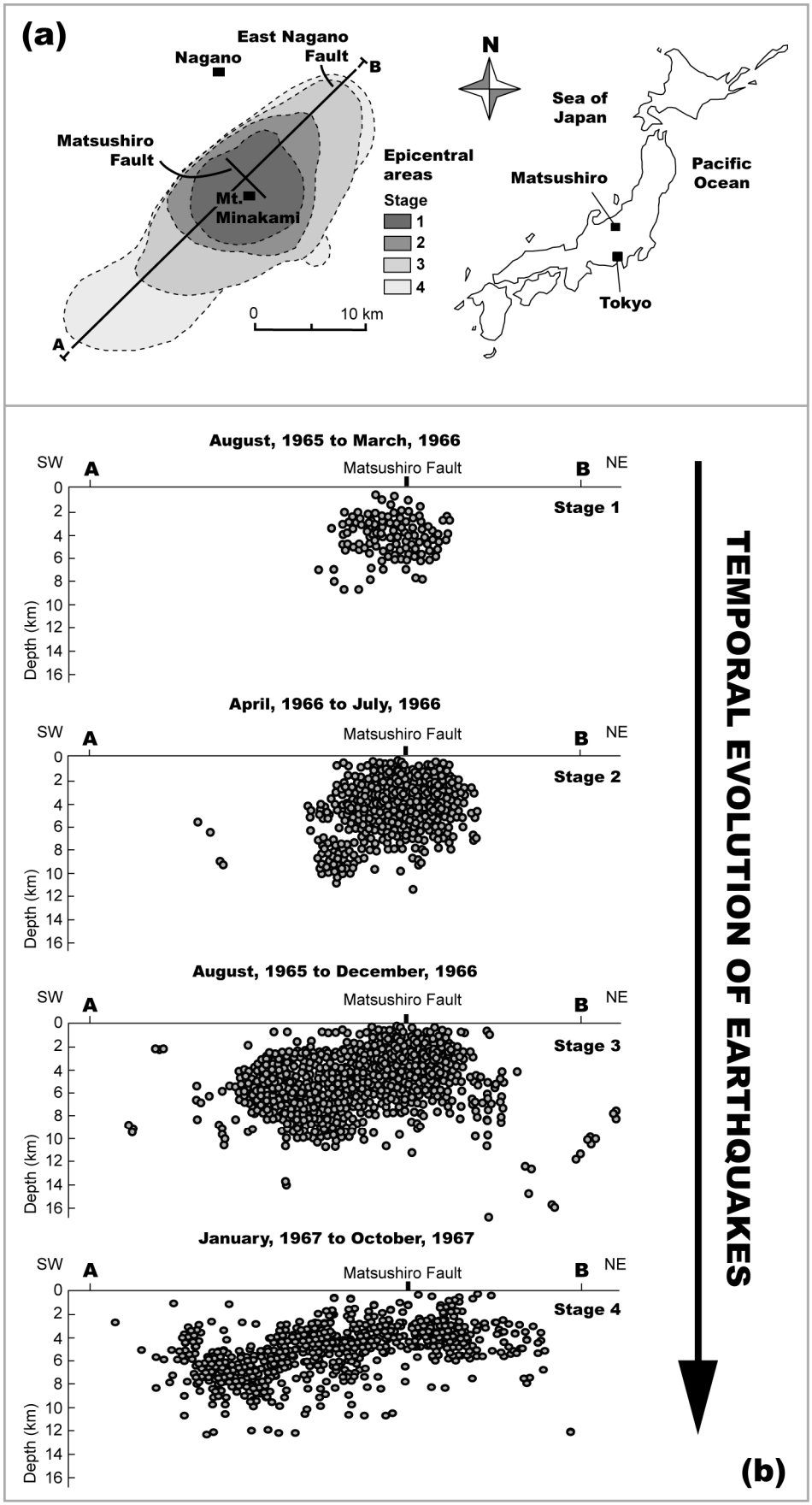
(a)
East Nagano
Fault
Nagano
B
A
Matsushiro
Fault
Mt.
Minakami
Epicentral
areas
Stage
1
2
3
4
0
10 km
N
Sea of
Japan
Pacific
Ocean
Matsushiro
Tokyo
August, 1965 to March, 1966
April, 1966 to July, 1966
August, 1965 to December, 1966
January, 1967 to October, 1967
SW
NE
Matsushiro Fault
Stage 1
Stage 2
Stage 3
Stage 4
Depth (km)
TEMPORAL EVOLUTION OF EARTHQUAKES
(b)

Figure 1

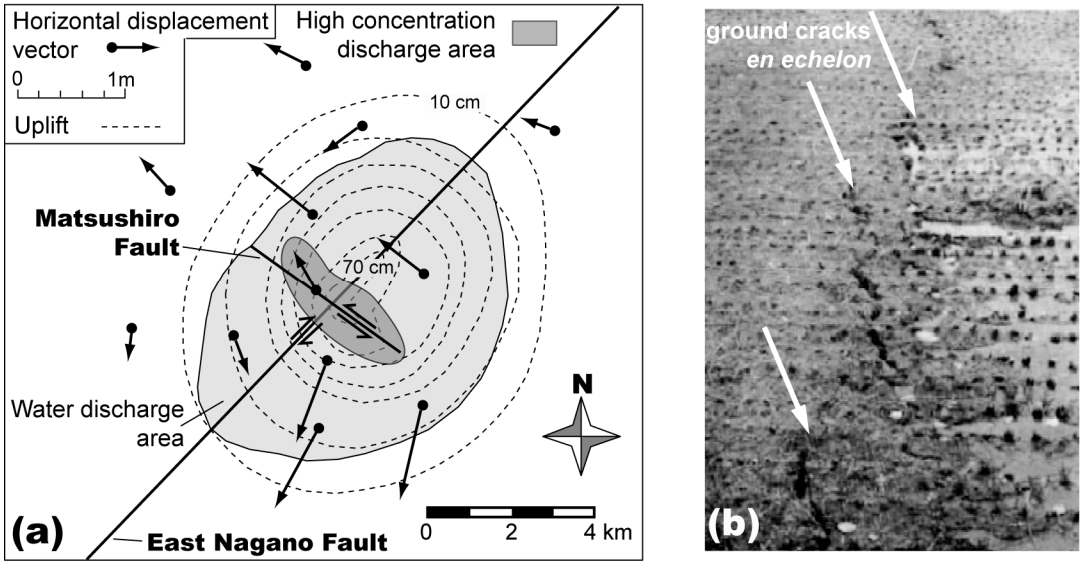
Horizontal displacement vector
0 1m
Uplift
High concentration discharge area
10 cm
70 cm
Matsushiro Fault
Water discharge area
N
(a)
East Nagano Fault
0 2 4 km
ground cracks en echelon
(b)

Figure 2

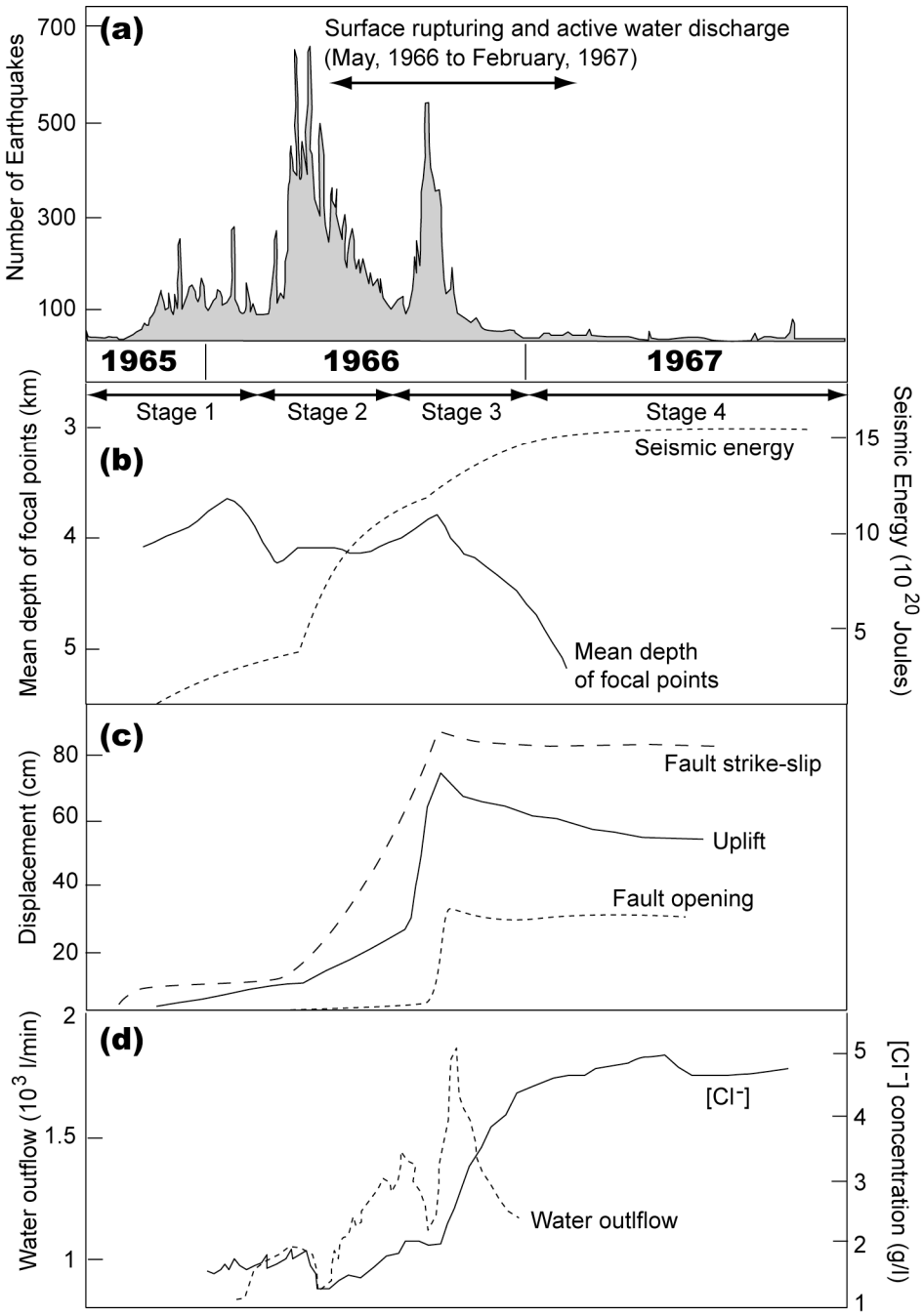
(a)
Surface rupturing and active water discharge
(May, 1966 to February, 1967)
Number of Earthquakes
700
500
300
100
1965
1966
1967
Stage 1
Stage 2
Stage 3
Stage 4
(b)
Seismic energy
Mean depth
of focal points
Mean depth of focal points (km)
Seismic Energy (10 20 Joules)
3
4
5
15
10
5
(c)
Fault strike-slip
Uplift
Fault opening
Displacement (cm)
80
60
40
20
2
(d)
[Cl-]
Water outlflow
Water outflow (10 3 l/min)
[Cl-] concentration (g/l)
2
1.5
1
5
4
3
2
1

Figure 3.

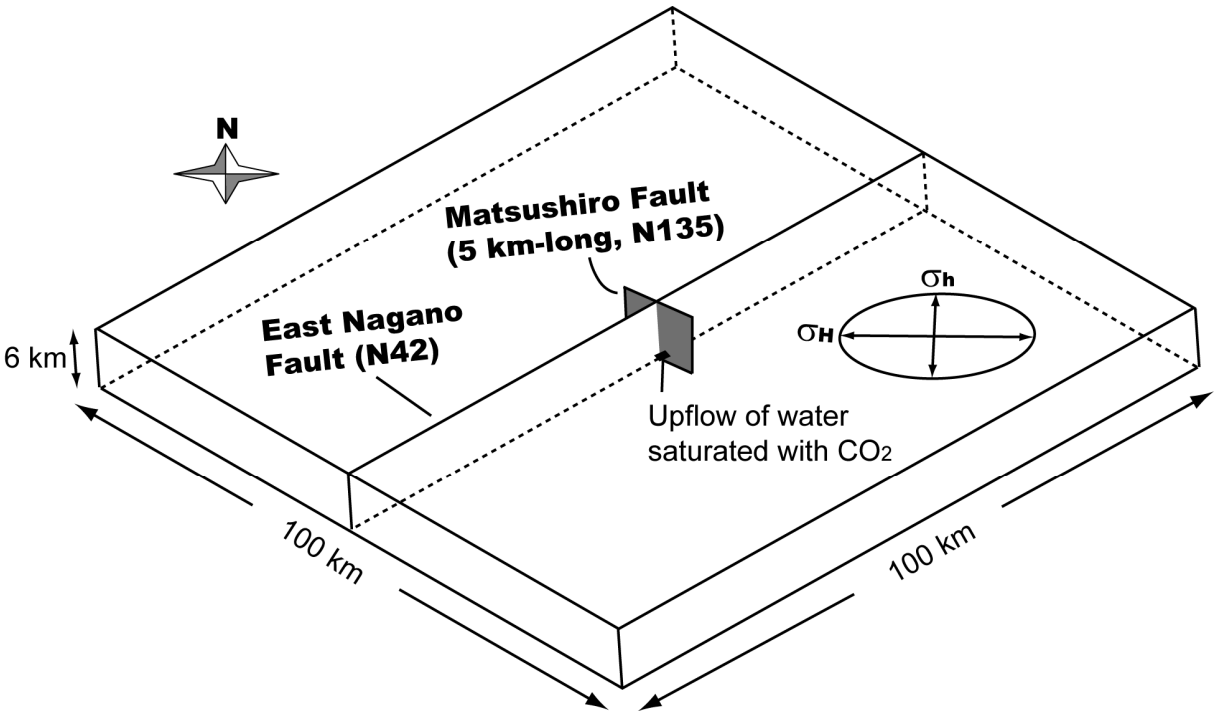
N
Matsushiro Fault
(5 km-long, N135)
East Nagano
Fault (N42)
σh
σH
6 km
Upflow of water
saturated with CO2
100 km
100 km

Figure 4

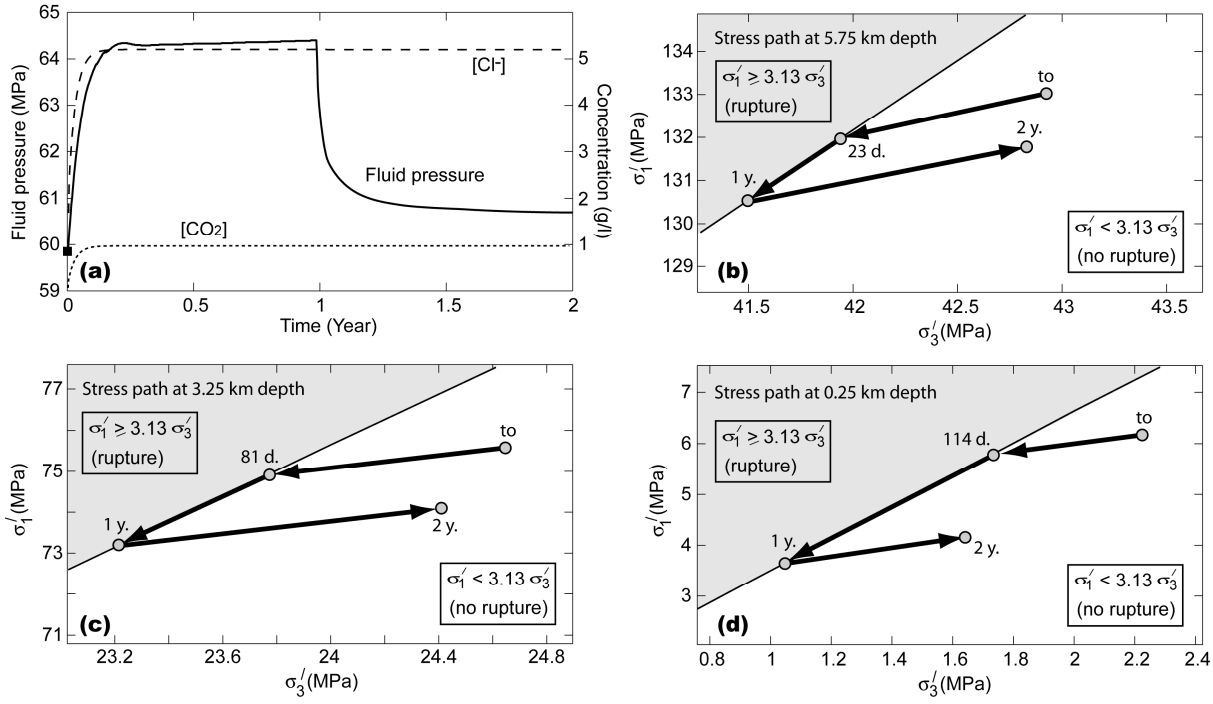
Fluid pressure (MPa)
Concentration (g/l)
Time (Year)
[Cl-]
Fluid pressure
[CO2]
(a)
Stress path at 5.75 km depth
σ1′ ≥ 3.13 σ3′
(rupture)
σ1′ < 3.13 σ3′
(no rupture)
to
2 y.
23 d.
1 y.
(b)
σ1′(MPa)
σ3′(MPa)
Stress path at 3.25 km depth
81 d.
(c)
Stress path at 0.25 km depth
114 d.
(d)

Figure 5

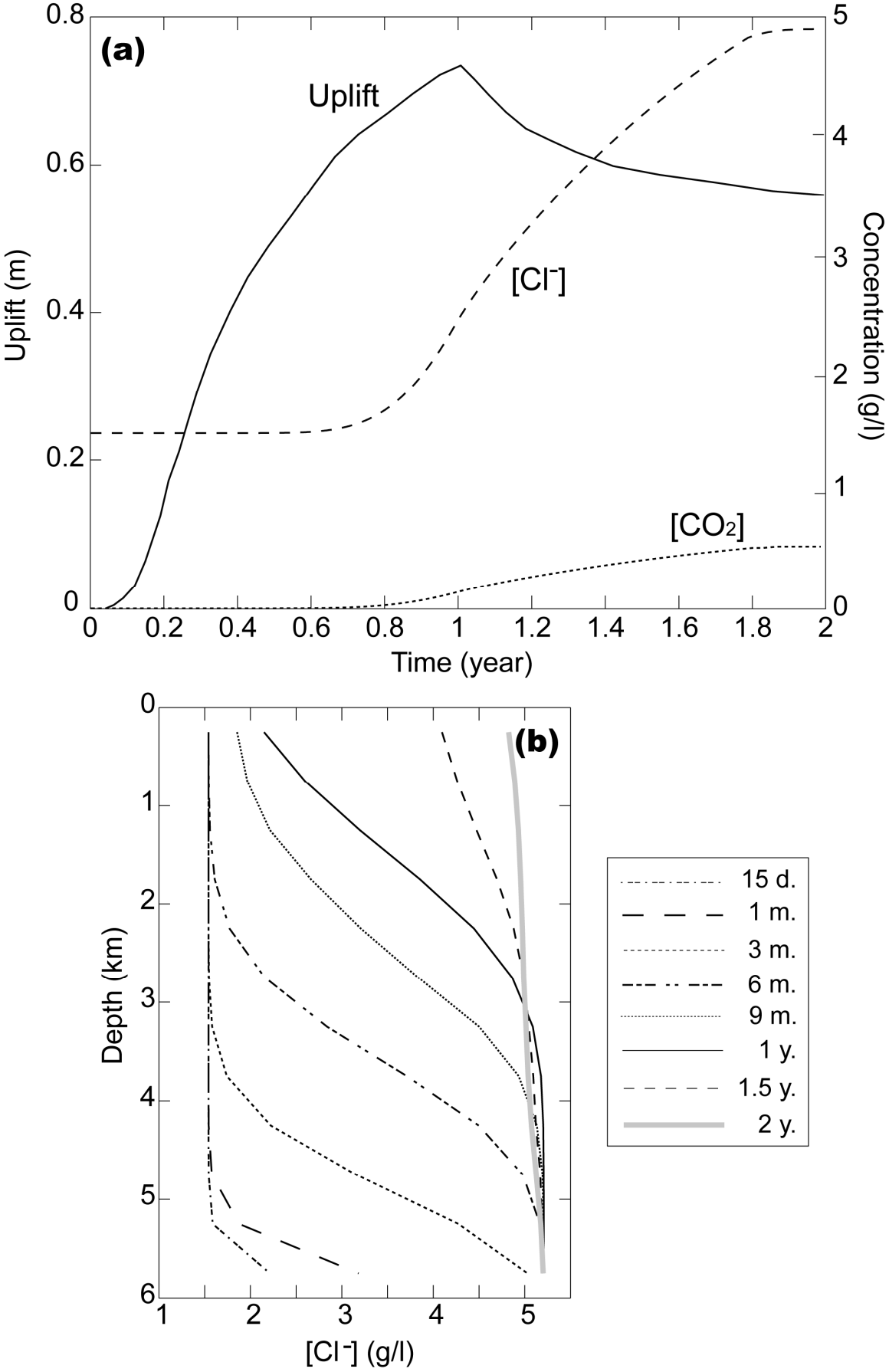
(a)
Uplift
[Cl⁻]
[CO2]
Uplift (m)
Concentration (g/l)
Time (year)
0
0.2
0.4
0.6
0.8
1
1.2
1.4
1.6
1.8
2
0
1
2
3
4
5
(b)
Depth (km)
[Cl⁻] (g/l)
15 d.
1 m.
3 m.
6 m.
9 m.
1 y.
1.5 y.
2 y.

Figure 6

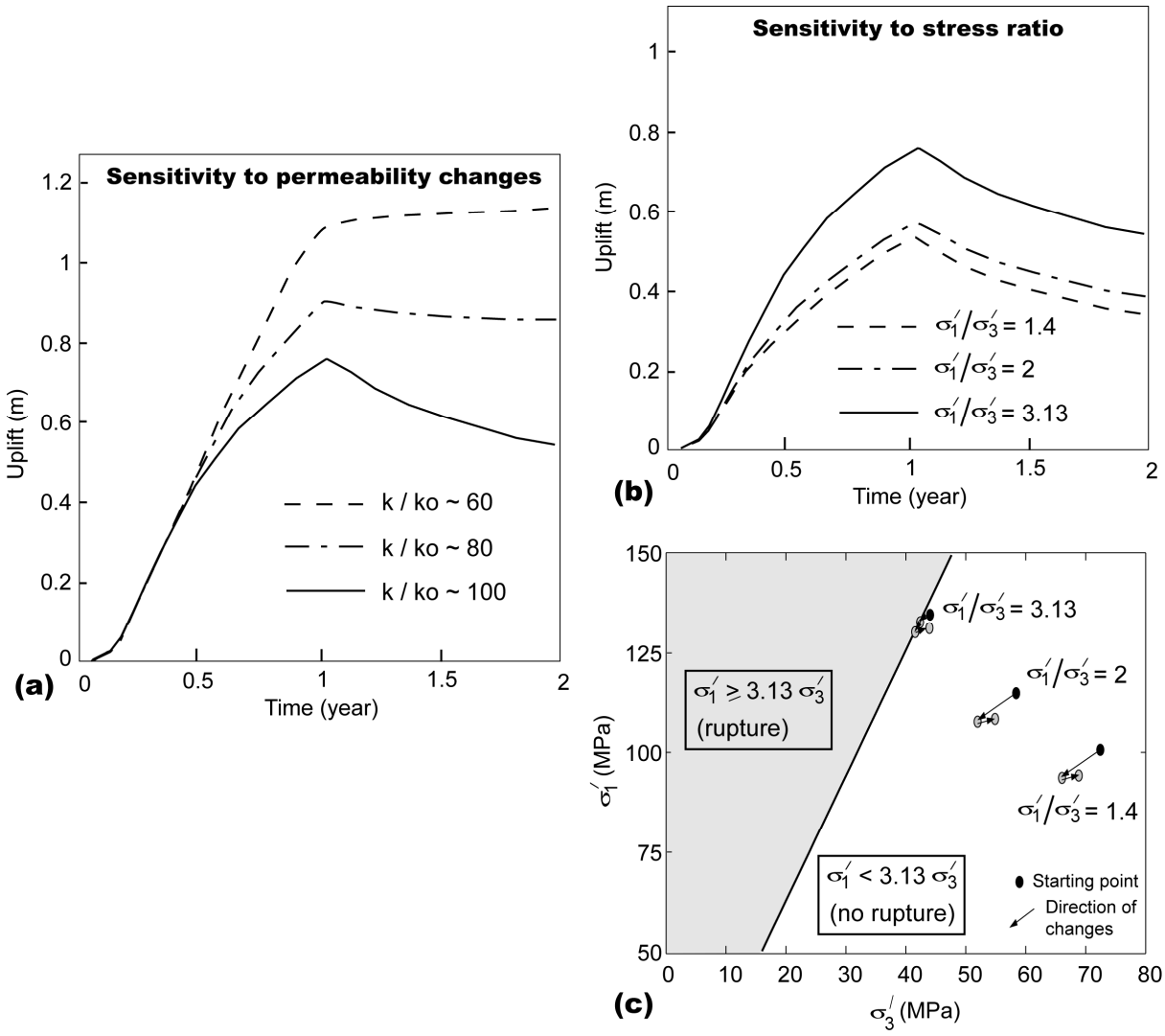
Sensitivity to permeability changes
Uplift (m)
Time (year)
k / ko ~ 60
k / ko ~ 80
k / ko ~ 100
(a)
Sensitivity to stress ratio
Uplift (m)
Time (year)
σ'1/σ'3 = 1.4
σ'1/σ'3 = 2
σ'1/σ'3 = 3.13
(b)
σ'1 (MPa)
σ'3 (MPa)
σ'1 ≥ 3.13 σ'3
(rupture)
σ'1 < 3.13 σ'3
(no rupture)
σ'1/σ'3 = 3.13
σ'1/σ'3 = 2
σ'1/σ'3 = 1.4
Starting point
Direction of changes
(c)

Figure 7

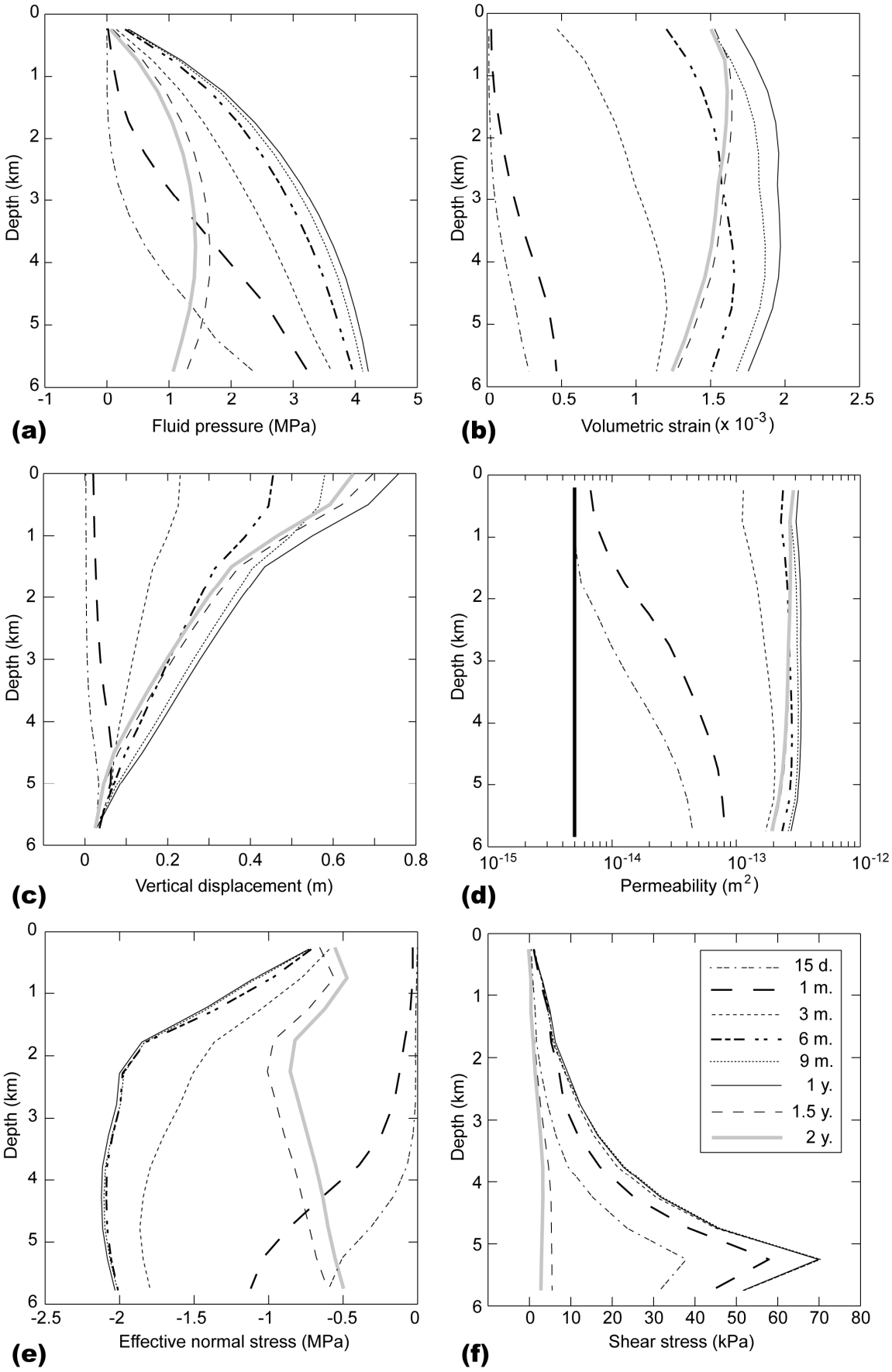
Depth (km)
Fluid pressure (MPa)
(a)
Volumetric strain (x 10^-3)
(b)
Vertical displacement (m)
(c)
Permeability (m^2)
(d)
Effective normal stress (MPa)
(e)
Shear stress (kPa)
(f)
15 d.
1 m.
3 m.
6 m.
9 m.
1 y.
1.5 y.
2 y.

Figure 8

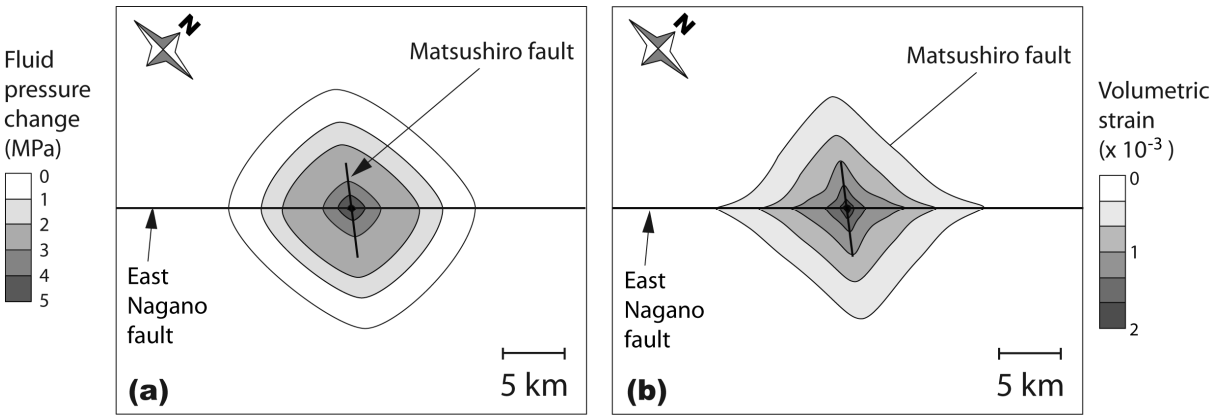
Fluid
pressure
change
(MPa)
0
1
2
3
4
5
N
Matsushiro fault
East
Nagano
fault
(a)
5 km
N
Matsushiro fault
East
Nagano
fault
(b)
5 km
Volumetric
strain
(x 10-3)
0
1
2

Figure 9

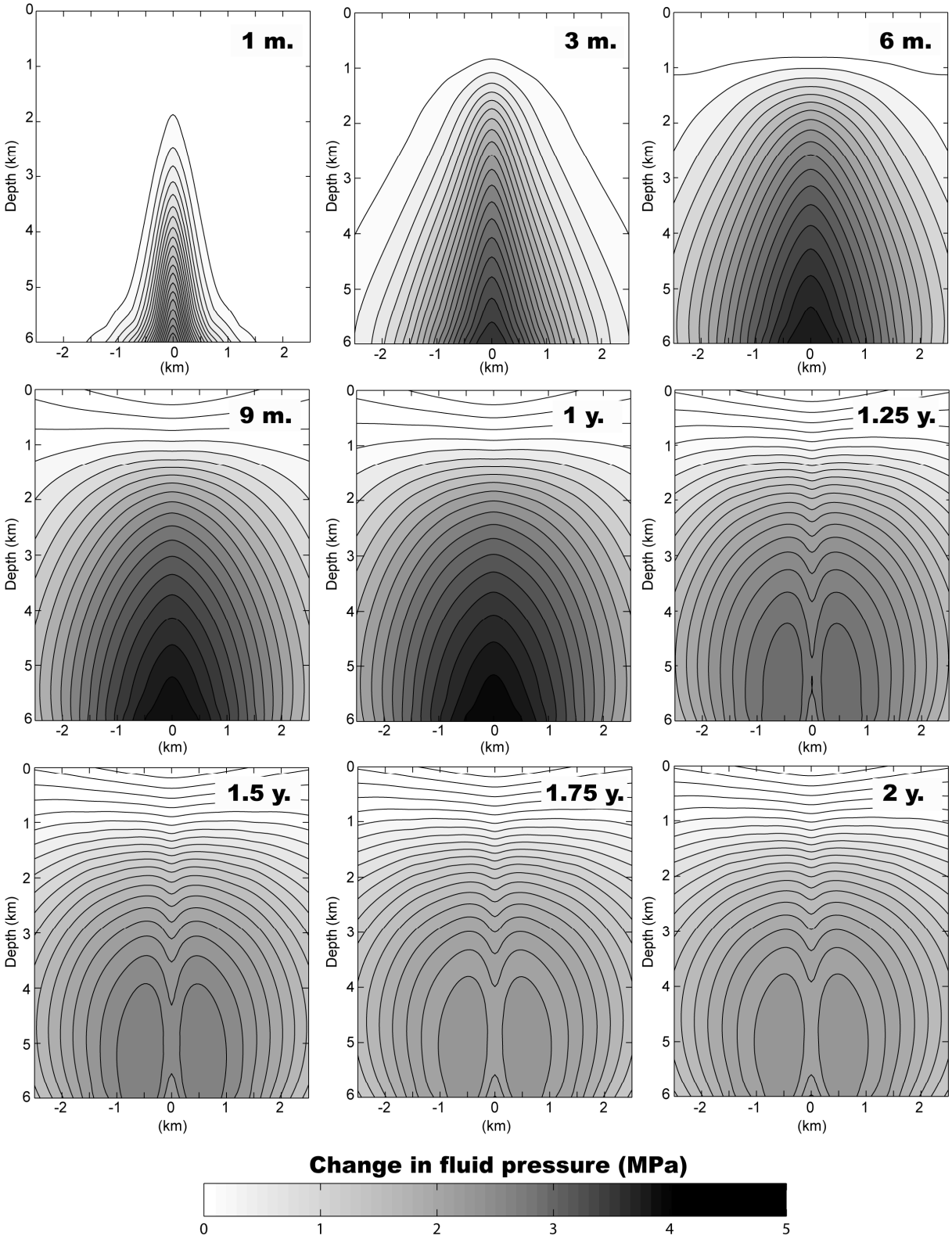
1 m.
3 m.
6 m.
9 m.
1 y.
1.25 y.
1.5 y.
1.75 y.
2 y.
Depth (km)
(km)
Change in fluid pressure (MPa)
0
1
2
3
4
5

Figure 10

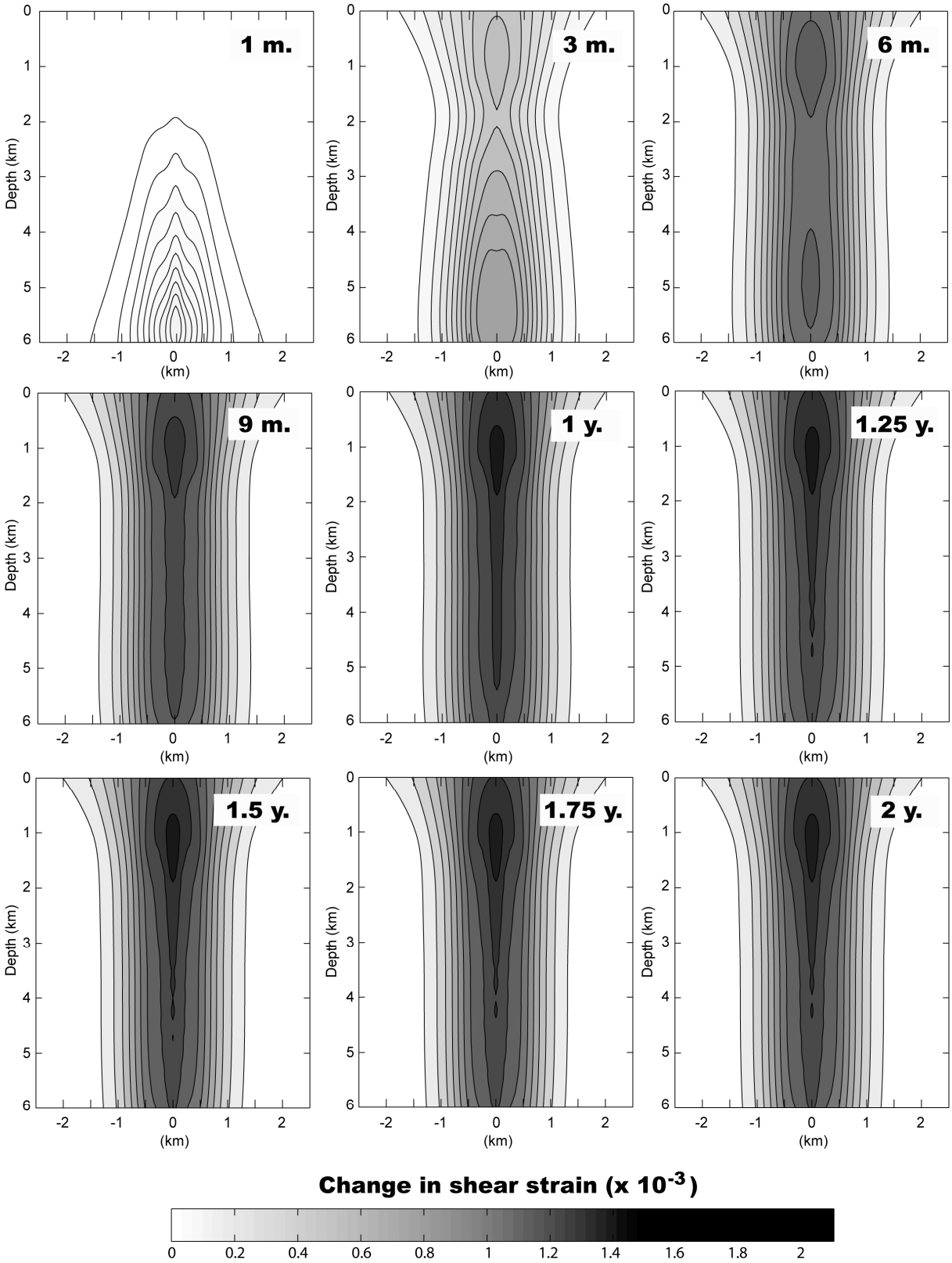
1 m.
3 m.
6 m.
9 m.
1 y.
1.25 y.
1.5 y.
1.75 y.
2 y.
Depth (km)
(km)
Change in shear strain (x 10-3)
0 0.2 0.4 0.6 0.8 1 1.2 1.4 1.6 1.8 2

Figure 11

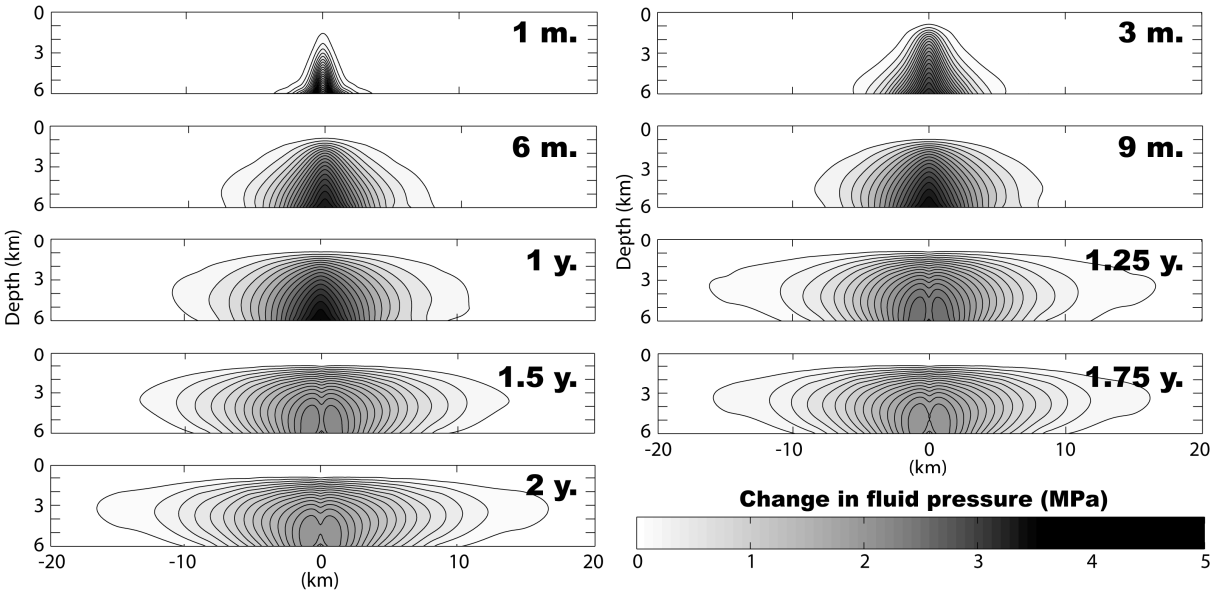
1 m.
3 m.
6 m.
9 m.
1 y.
1.25 y.
1.5 y.
1.75 y.
2 y.
Depth (km)
(km)
Change in fluid pressure (MPa)

Figure 12

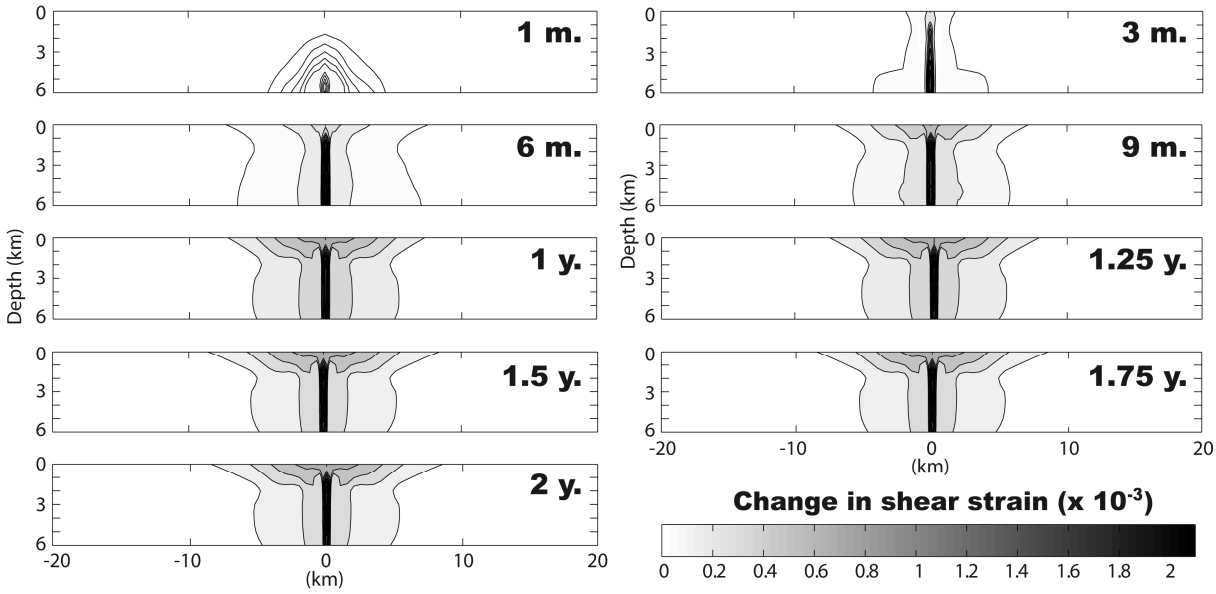
1 m.
3 m.
6 m.
9 m.
1 y.
1.25 y.
1.5 y.
1.75 y.
2 y.
Depth (km)
0
3
6
-20
-10
0
10
20
(km)
Change in shear strain (x 10-3)
0
0.2
0.4
0.6
0.8
1
1.2
1.4
1.6
1.8
2

Figure 13

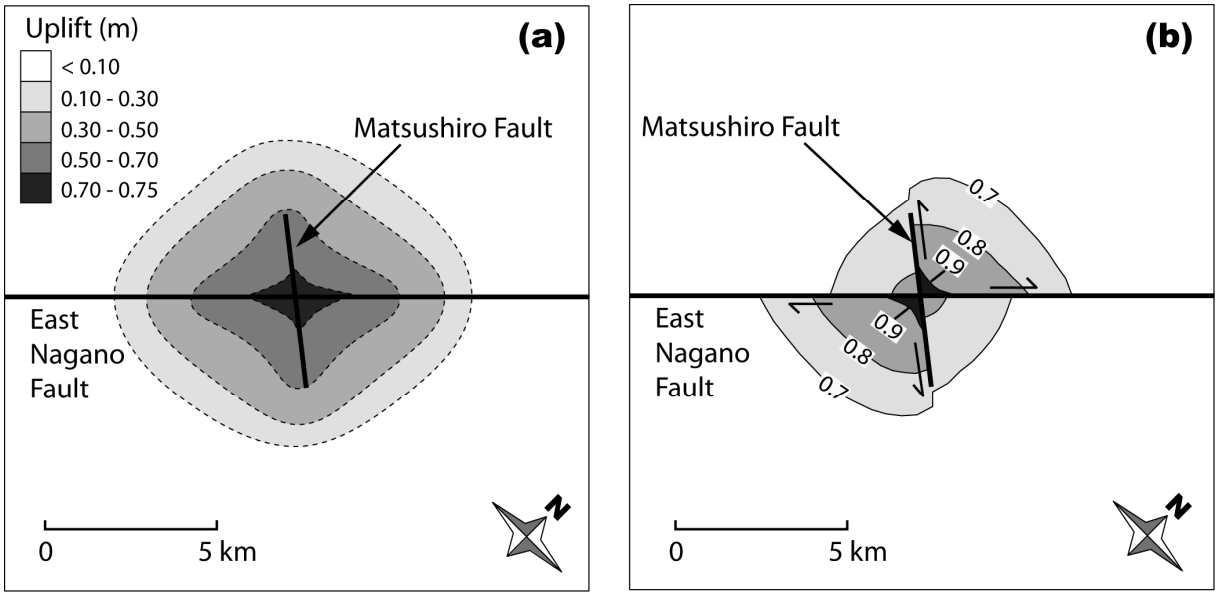
Uplift (m)
< 0.10
0.10 - 0.30
0.30 - 0.50
0.50 - 0.70
0.70 - 0.75
(a)
Matsushiro Fault
East
Nagano
Fault
0
5 km
N
(b)
Matsushiro Fault
0.7
0.8
0.9
East
Nagano
Fault
0.9
0.8
0.7
0
5 km
N

Figure 14

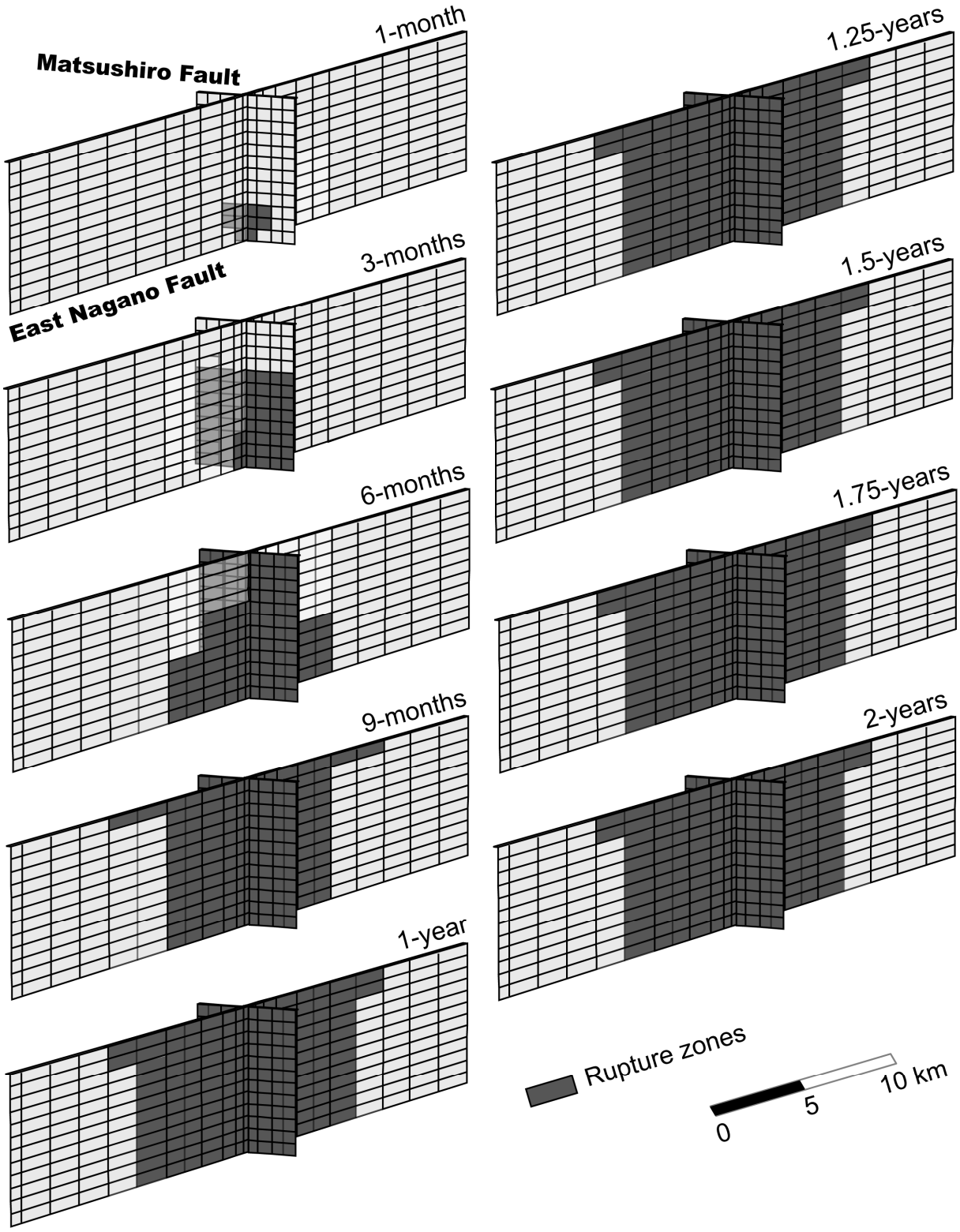
Matsushiro Fault
East Nagano Fault
1-month
3-months
6-months
9-months
1-year
1.25-years
1.5-years
1.75-years
2-years
Rupture zones
0
5
10 km

Figure 15